The Plant Cell, Vol. 31: 1807–1828, August 2019, www.plantcell.org © 2019 ASPB.

TTL Proteins Scaffold Brassinosteroid Signaling Components at the Plasma Membrane to Optimize Signal Transduction in Arabidopsis

Vítor Amorim-Silva,[a] Álvaro García-Moreno,[a] Araceli G. Castillo,[b] Naoufal Lakhssassi,[c] Alicia Esteban del Valle,[a] Jessica Pérez-Sancho,[a] Yansha Li,[d] David Posé,[a] Josefa Pérez-Rodriguez,[a] Jinxing Lin,[e] Victoriano Valpuesta,[a] Omar Borsani,[f] Cyril Zipfel,[g,h] Alberto P. Macho,[d,g] and Miguel A. Botella[a,1]

[a] Departamento de Biología Molecular y Bioquímica, Instituto de Hortofruticultura Subtropical y Mediterránea "La Mayora," Universidad de Málaga-Consejo Superior de Investigaciones Científicas (IHSM-UMA-CSIC), Universidad de Málaga, Campus Teatinos, 29071 Málaga, Spain

[b] Departamento de Biología Celular, Genética y Fisiología, Instituto de Hortofruticultura Subtropical y Mediterránea "La Mayora," Universidad de Málaga-Consejo Superior de Investigaciones Científicas (IHSM-UMA-CSIC), Universidad de Málaga, Campus Teatinos, 29071 Málaga, Spain

[c] Department of Plant, Soil and Agricultural Systems, Southern Illinois University, Carbondale, Illinois 62901

[d] Shanghai Center for Plant Stress Biology, CAS Center for Excellence in Molecular Plant Sciences, Shanghai Institutes of Biological Sciences, Chinese Academy of Sciences (CAS), Shanghai, China

[e] College of Biological Sciences and Technology, Beijing Forestry University, Beijing 100083, China

[f] Departamento de Biología Vegetal, Laboratorio de Bioquímica, Facultad de Agronomía Universidad de la República, Montevideo, Uruguay

[g] The Sainsbury Laboratory, University of East Anglia, Norwich Research Park, Norwich, NR4 7UH, United Kingdom

[h] Institute of Plant and Microbial Biology and Zurich-Basel Plant Science Center, University of Zurich, CH-8008 Zurich, Switzerland

ORCID IDs: 0000-0002-3978-7205 (V.A.-S.); 0000-0001-7007-998X (Á.G.-M.); 0000-0003-3990-5475 (A.G.C.); 0000-0002-8255-9419 (N.L.); 0000-0003-3039-1172 (A.E.d.V.); 0000-0002-6201-3240 (J.P.-S.); 0000-0002-4864-9461 (Y.L.); 0000-0003-3332-4661 (D.P.); 0000-0003-1676-2053 (J.P.-R.); 0000-0001-9338-1356 (J.L.); 0000-0003-0922-6615 (V.V.); 0000-0002-9111-5801 (O.B.); 0000-0003-4935-8583 (C.Z.); 0000-0001-9935-8026 (A.P.M.); 0000-0002-8867-1831 (M.A.B.)

Brassinosteroids (BRs) form a group of steroidal hormones essential for plant growth, development, and stress responses. BRs are perceived extracellularly by plasma membrane receptor-like kinases that activate an interconnected signal transduction cascade, leading to the transcriptional regulation of BR-responsive genes. *TETRATRICOPEPTIDE THIOREDOXIN-LIKE* (*TTL*) genes are specific for land plants, and their encoded proteins are defined by the presence of protein–protein interaction motives, that is, an intrinsic disordered region at the N terminus, six tetratricopeptide repeat domains, and a C terminus with homology to thioredoxins. TTL proteins thus likely mediate the assembly of multiprotein complexes. Phenotypic, molecular, and genetic analyses show that TTL proteins are positive regulators of BR signaling in Arabidopsis (*Arabidopsis thaliana*). TTL3 directly interacts with a constitutively active BRASSINOSTEROID INSENSITIVE1 (BRI1) receptor kinase, BRI1-SUPPRESSOR1 phosphatase, and the BRASSINAZOLE RESISTANT1 transcription factor and associates with BR-SIGNALING KINASE1, BRASSINOSTEROID INSENSITIVE2 kinases, but not with BRI1-ASSOCIATED KINASE1. A functional TTL3-green fluorescent protein (GFP) shows dual cytoplasmic plasma membrane localization. Depleting the endogenous BR content reduces plasma membrane localization of TTL3-GFP, while increasing BR content causes its plasma membrane relocalization, where it strengthens the association of BR signaling components. Our results reveal that TTL proteins promote BR responses and suggest that TTL proteins may function as scaffold proteins by bringing together cytoplasmic and plasma membrane BR signaling components.

INTRODUCTION

Brassinosteroids (BRs) are a family of growth-promoting hormones with essential roles in a wide range of developmental and physiological processes (Belkhadir and Jaillais, 2015; Chaiwanon et al., 2016; Jaillais and Vert, 2016). However, in addition to their well-established function in growth, essential roles in the trade-off between growth and tolerance to biotic and abiotic stress episodes are now being unveiled (Lozano-Durán and Zipfel, 2015; Zhang et al., 2016; Nolan et al., 2017; Tian et al., 2018). BRs are perceived at the plasma membrane by ligand-induced heterodimers of the receptor kinases BRASSINOSTEROID INSENSITIVE1 (BRI1) and SOMATIC EMBBRYOGENESIS RECEPTOR KINASE (SERK) protein family members, which activates an interconnected signal transduction cascade, leading to the transcriptional

[1] Address correspondence to: mabotella@uma.es.
The author responsible for distribution of materials integral to the findings presented in this article in accordance with the policy described in the Instructions for Authors (www.plantcell.org) is: Miguel A. Botella (mabotella@uma.es).
www.plantcell.org/cgi/doi/10.1105/tpc.19.00150

IN A NUTSHELL

Background: The plant hormone Brassinosteroid (BR) is essential for proper growth. This hormone is extracellularly perceived by plasma membrane Receptor Like-Kinases, causing transphosphorylation of their cytosolic domains and the subsequent phosphorylation/dephosphorylation of signaling components. These events lead to the activation of key transcription factors, which in turn activate the transcription of multiple genes that enhance plant growth. Although most of the core signaling components have been identified, we know little about how these components associate to optimize signaling.

Question: We previously observed that the plant-specific *TETRATRICOPEPTIDE THIOREDOXIN-LIKE* (*TTL*) genes, whose encoded proteins contain protein–protein interaction domains, are involved in abiotic stress tolerance. In this work, we aimed to determine whether these proteins are positive regulators of BR signaling and could serve as a scaffold of BR components to optimize signaling.

Findings: We found that mutations in these *TTL* genes caused marked defects in BR responses. Protein interaction studies indicate that TTL proteins either interact or associate *in vivo* with most core BR signaling components. Cellular studies of Arabidopsis plants transformed with a functional TTL3-GFP protein indicate that while TTL3-GFP is mainly localized at the cytosol, treatment with exogenous BR caused an increased localization of this protein at the plasma membrane. On the other hand, reducing the amount of endogenous BR caused dissociation of TTL3-GFP from the plasma membrane. Furthermore, expression of TTL3 strongly increased the plasma membrane association of a plasma membrane and a cytoplasmic BR signaling component. Taking all this together, we propose that TTLs function as a scaffold that increases the concentration of BR components at the plasma membrane and thereby optimizes BR signaling.

Next steps: Our work has shown that *TTL* genes, which were initially identified as having a role in salt tolerance based on genetic studies, function in BR responses. Whether their contribution to salt tolerance is mediated by their role in BR signaling, in other signaling pathways, or as scaffolding components remains to be established. Genetic determinants with a role in growth and stress tolerance may have important biotechnological applications, particularly considering that *TTL* genes are conserved in all major crops.

regulation of BR-responsive genes (Belkhadir and Jaillais, 2015). BRI1 KINASE INHIBITOR1 dissociates from activated BRI1, which phosphorylates the BR-SIGNALING KINASE (BSK) family proteins BSK1 and BSK3 and the CONSTITUTIVE DIFFERENTIAL GROWTH1, which in turn activate the BRI1-SUPPRESSOR1 (BSU1) phosphatase (Wang et al., 2014; Belkhadir and Jaillais, 2015; Ren et al., 2019). Next, the active (phosphorylated) BSU1 leads to dephosphorylation and inactivation of the glycogen synthase kinase3 (GSK3)–like BRASSINOSTEROID INSENSITIVE2 (BIN2). In the absence of BRs, BIN2 is active and phosphorylates the two homologous transcription factors BRASSINAZOLE RESISTANT1 (BZR1) and BRI1-ETHYL METHANESULFONATE SUPPRESSOR1 (BES1/BZR2), which results in their inactivation and degradation (Wang et al., 2014; Belkhadir and Jaillais, 2015). By contrast, when BR is present, BIN2 is inactivated and degraded by the proteasome mediated by the F-box E3 ubiquitin ligase KINK SUPPRESSED1 in *bzr1-1D* (Zhu et al., 2017), leading to both the stabilization and the activation of BZR1 and BES1 and therefore to transcriptional regulation of BR-responsive genes (Wang et al., 2014; Belkhadir and Jaillais, 2015).

In Arabidopsis (*Arabidopsis thaliana*), the *TETRATRICOPEPTIDE THIOREDOXIN-LIKE* (*TTL*) gene family is composed of four members (*TTL1* to *TTL4*) and mutations in *TTL1*, *TTL3*, and *TTL4* cause reduced growth under abiotic stresses such as salinity and drought (Rosado et al., 2006; Ceserani et al., 2009; Lakhssassi et al., 2012). This stress hypersensitivity is exacerbated in double and triple *ttl* mutants (Lakhssassi et al., 2012). *TTL2* is specifically expressed in pollen grains and does not have a role in stress tolerance, but it is important for male sporogenesis (Lakhssassi et al., 2012). *TTL* genes encode proteins with a common modular architecture containing six tetratricopeptide repeat (TPR) domains distributed in specific positions throughout the sequence and a C-terminal sequence with homology to thioredoxins (Rosado et al., 2006; Lakhssassi et al., 2012). TPR domains are well-described protein–protein interaction modules; however, how TTL proteins function mechanistically in stress tolerance remains elusive.

Several lines of circumstantial evidence point to a role of TTL proteins in BR responses, which open the possibility of a direct link between stress tolerance and BR signaling by the TTL proteins. First, the TTL3 protein, whose gene is the most highly expressed among the *TTL* gene family, was identified as an interacting partner of the activated (phosphorylated) cytoplasmic domain of VASCULAR HIGHWAY1/BRI1-LIKE RECEPTOR KINASE2 (BRL2). BRL2 has a role in vascular development and belong to the BRI family (Ceserani et al., 2009), although BRL2 cannot bind BRs (Belkhadir and Jaillais, 2015). Second, a *ttl3* mutant showed altered growth in the presence of exogenous BRs (Ceserani et al., 2009). Third, TTL proteins are predicted to interact and function as co-chaperones of Hsp90 (Prasad et al., 2010), which has been recently identified to have important roles in BR signaling by interacting with specific BR signaling components (Lachowiec et al., 2013; Samakovli et al., 2014; Shigeta et al., 2014, 2015). Fourth, a triple Arabidopsis line with T-DNA insertions in *TTL1*, *TTL3*, and *TTL4* shows defects in vasculature development and male sporogenesis, hallmarks of BR-defective mutants (Yang et al., 2011; Lakhssassi et al., 2012). Finally, *TTL1*, *TTL3*, and *TTL4* are specifically induced by BR application, but not by other hormones (Prasad et al., 2010).

Based on phenotypic, molecular, and genetic analyses, we show that *TTL1*, *TTL3*, and *TTL4* genes, in addition to their reported role in abiotic stress tolerance, are positive regulators of BR signaling. The well-described TPR protein interaction modules of TTL proteins and their role in the assembly of multiprotein complexes (Blatch and Lässle, 1999; D'Andrea and Regan, 2003; Yang et al., 2005) led us to hypothesize that these proteins could function as a scaffold for BR signaling. Indeed, we show that TTL3 interacts with constitutively active BRI1, BSU1, and BZR1 and associates in vivo with most BR signaling components, with the exception of BRI1-ASSOCIATED KINASE1 (BAK1). We also show that a functional TTL3 tagged with a green fluorescent protein (GFP) shows a dual cytoplasmic and plasma membrane localization that is dependent on endogenous BR content. Furthermore, TTL3 greatly enhances the interaction between BSK1 and BZR1 at the plasma membrane and suppresses the BIN2-promoted cytoplasmic retention of BZR1-GFP. Together, we reveal that TTL proteins function as positive regulators of BR signaling, likely by bringing together signaling components at the plasma membrane.

RESULTS

Interaction Analysis of TTL3 with BRI1

The TTL3 protein, also known as VH1-interacting TPR-containing protein, has been identified as an interactor of the activated (phosphorylated) cytoplasmic domain of BRL2 (Ceserani et al., 2009), a receptor kinase of the BRI1 family with a role in vascular development (Caño-Delgado et al., 2004; Ceserani et al., 2009). *TTL3* belongs to a family of four genes (*TTL1* to *TTL4*) in Arabidopsis (Rosado et al., 2006; Lakhssassi et al., 2012). While *TTL1*, *TTL3*, and *TTL4* show ubiquitous expression, *TTL2* expression is restricted to pollen grains. We confirmed the reported defects in vein formation using a different *ttl3* mutant allele (Supplemental Figure 1A) and showed that mutations in *TTL1* and *TTL4*, but not *TTL2*, also caused venation defects that were markedly enhanced in a triple *ttl1 ttl3 tt4* mutant (hereafter *ttl134*; Supplemental Figure 1A).

TTL3 has been proposed to be an adaptor protein of BRL2 that, through association with other proteins, modulates vein formation (Ceserani et al., 2009). TTL3, as for other TTL proteins from other plant species (Rosado et al., 2006; Lakhssassi et al., 2012), is characterized by the presence of six TPRs and a C-terminal domain with homology to thioredoxins. An in silico structural analysis of TTL3 predicts the presence of an intrinsically disordered region (IDR) at the N terminus (Supplemental Figure 2) with the rest of the protein forming a horseshoe-shaped structure composed of multiple helix-turn-helix motifs (Figure 1A). This structure is consistent with TTL3 being involved in protein–protein interactions and the assembly of multiprotein complexes (Blatch and Lässle, 1999; D'Andrea and Regan, 2003; Yang et al., 2005).

The similarity between BRL2 and BRI1 kinase domains (Supplemental Figure 3) suggested that TTL3 could also interact with the BRI1 cytoplasmic domain. We therefore tested the direct interaction of TTL3 with the BRI1 cytoplasmic region that includes the juxta-membrane (JM), the kinase domain, and the carboxy-terminal (CT) domain (BRI1cyt; Figure 1B). While BRI1cyt was soluble when fused to an maltose binding protein (MBP) tag (Supplemental Figure 4), we were unable to produce full-length TTL3 protein fused to glutathione S-transferase (GST) despite many attempts. This low stability was probably caused by the presence of the IDR (Habchi et al., 2014). Accordingly, we produced in *Escherichia coli* two different fragments: TTL3 lacking the N terminus IDR (TTL3ΔN1) and TTL3 containing the TRLX domain (TTL3ΔN3; Figure 1C; Supplemental Figure 4). Using an in vitro GST pull-down assay, we did not detect an interaction between BRI1cyt and either TTL3ΔN1 or TTL3ΔN3 (Figures 1C and 1D). Because the activation of BRI1 is dependent on BAK1 transphosphorylation on specific residues at the JM and CT (Wang et al., 2008), we next used a BAK1-independent BRI1 constitutively active (phosphomimetic) form BRI1cyt^{JMCT9D}. In this mutant version, nine Ser and Thr have been substituted by Asp at the juxtamembrane (JM) andcarboxy-region CR domains (Figure 1B; Wang et al., 2008). In this case, BRI1cyt^{JMCT9D} was pulled down by TL3ΔN1, but not by TTL3ΔN3 (Figures 1C and 1D). This indicates that TTL3 predominantly interacts with active BRI1 and that this interaction occurs through the TPR domains, but not the thioredoxin-like (TRXL) domain of TTL3.

Next, we investigated this interaction in vivo by performing co-immunoprecipitation (Co-IP) assays after transient expression of tagged full-length TTL3 and BRI1 in *Nicotiana benthamiana*. After immunoprecipitation of GFP-TTL3 and free GFP using GFP-Trap beads, we detected a strong specific interaction between GFP-TTL3 and BRI1-HA (Figure 1E). Additional Co-IP experiments using a C-terminal GFP-tagged TTL3 protein (TTL3-GFP) coexpressed with C-terminal hemagglutinin (HA)-tagged BRI1 protein (BRI1-HA; Supplemental Figure 5A) and BRI1-GFP coexpressed with TTL3-HA (Supplemental Figure 5B) further confirmed the TTL3-BRI1 interaction and indicated that the position and tag used in the Co-IP experiments does not affect their in planta interaction.

We further used Co-IP assays to map the TTL3 domains required for the interaction with BRI1. We performed this analysis in planta to determine the possible role of the IDR domain in the interaction, which was not possible using in vitro assays. We generated a series of truncated TTL3 fragments with deletions at the N terminus (TTL3ΔN1, TTL3ΔN2, TTL3ΔN3) and at the C terminus (TTL3ΔC1, TTL3ΔC2; Figure 1C), transcriptionally fused these fragments to GFP at the N terminus, and coexpressed these constructs with BRI1-HA in *N. benthamiana* leaves. All expressed proteins showed the expected molecular size (Figure 1E, input). TTL3ΔC1 and TTL3ΔC2 truncated proteins, both lacking the TRLX domain, showed lower accumulation than the others (Figure 1E, input), suggesting that TRLX is important for protein stabilization.

The full-length TTL3 and three of the five truncated TTL3 proteins, that is, GFP-TTL3ΔN1, GFP-TTL3ΔN2, and GFP-TTL3ΔC2, which all having in common TPR3 to TPR6 (Figure 1C), co-immunoprecipitated (CoIP) BRI1-HA with different efficiency, indicating that these domains are essential for the interaction, which is consistent with the in vitro data (Figure 1D). To quantify the interaction of the different TTL protein fragments and BRI1, the amount of CoIP BRI1-HA was normalized relative to the amount of protein input (Figure 1E). The strongest interaction occurs with the full-length TTL3 protein, indicating that all domains contribute to stabilize the interaction with BRI1. A lower but similar interaction

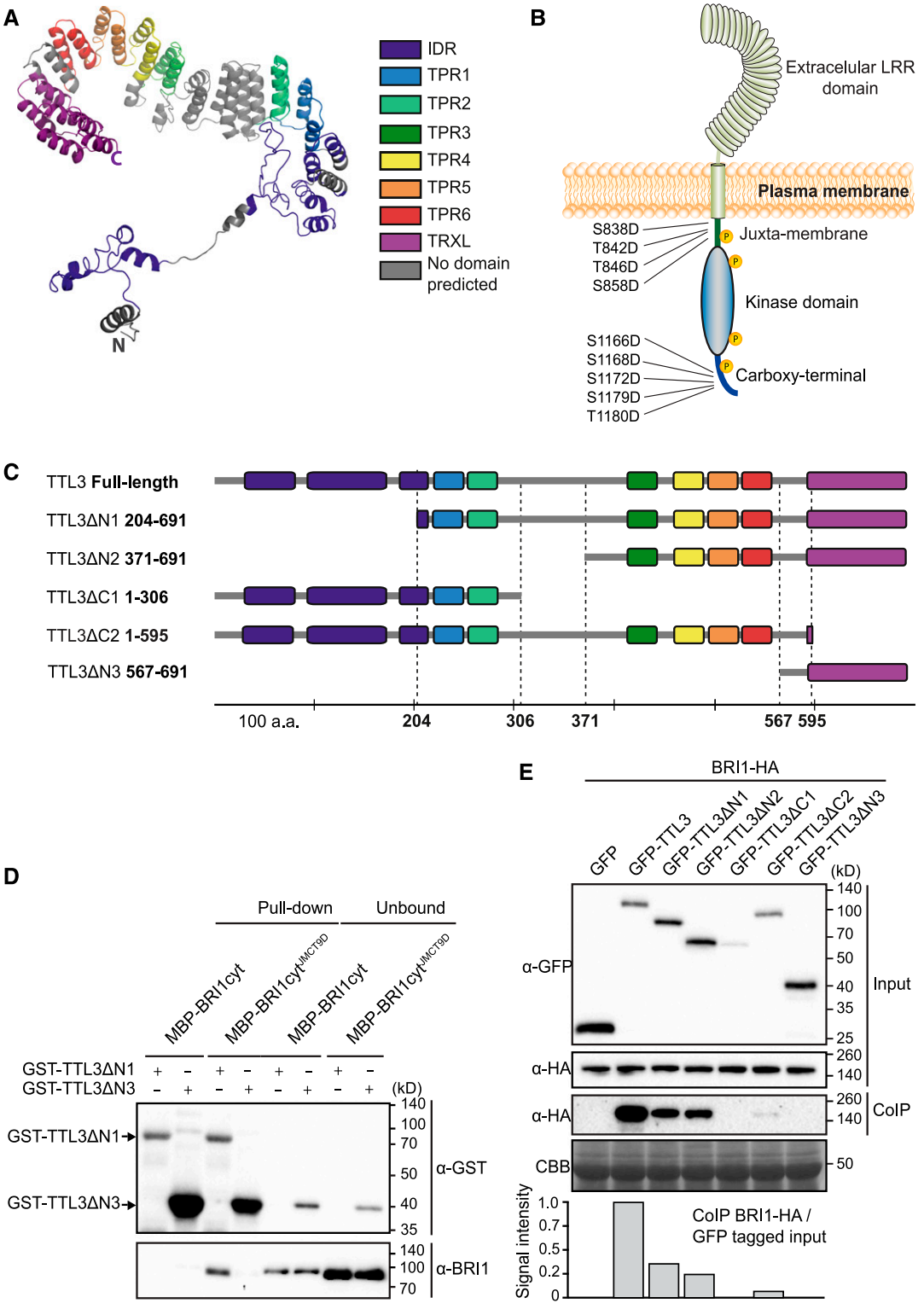

Figure 1. TTL3 Interacts with BRI1 In Vivo and In Vitro.

(A) Structural model of TTL3 protein predicted in silico using I-TASSER server (Zhang, 2008) and processed by PyMOL (Schrödinger). C, C terminus; N, N terminus.

was observed with GFP-TTL3ΔN1 and GFP-TTL3ΔN2, both containing the TRLX domain, indicating that this domain is important for stabilizing the interaction, but is not sufficient for the in vitro or in vivo interaction with BRI1 (Figures 1C and 1E). Consistent with this, removing the TRLX region in GFP-TTL3ΔC2 greatly reduced the interaction between TTL3 and BRI1 (Figures 1C to 1E).

Finally, the interaction between BRI1 and TTL3 was also investigated using bimolecular fluorescence complementation (BiFC) assays in *N. benthamiana* leaves, which provide additional information about the subcellular localization of the interaction. Coexpression of the TTL3-N-terminal half of YFP (nYFP) with the BRI1-C-terminal half of YFP (cYFP) or BRI1-nYFP with TTL3-cYFP (Supplemental Figure 6) reconstituted functional YFP proteins at the plasma membrane, confirming the interaction and consistent with the plasma membrane localization of BRI1.

BAK1, also known as SERK3, and other SERK proteins are transmembrane kinases that function as BR coreceptors (Ma et al., 2016). Similar Co-IP experiments using TTL3-GFP and BAK1 transiently coexpressed in *N. benthamiana* indicated that, contrary to BRI1, TTL3 does not associate in vivo with BAK1 (Supplemental Figure 5C). This result was verified by BiFC assays in *N. benthamiana* leaves since confocal microscopy analyses revealed that coexpression of TTL3-nYFP with BAK1-cYFP (Supplemental Figure 6A) and also BAK1-nYFP with TTL3-cYFP (Supplemental Figure 6B) did not reconstitute functional YFP proteins. To confirm that BiFC BAK1 constructs were functional, we performed a BiFC between BRI1 and BAK1 and observed weak but positive signals (Supplemental Figures 6A and 6B)

TTL Proteins Play a Positive Role in BR Signaling

The interaction of TTL3 with BRI1 supports a role for TTL3 in BR signaling. Furthermore, previous expression analyses indicate that *TTL1*, *TTL3*, and *TTL4* transcripts are induced by BR (Prasad et al., 2010), which is also supported by public transcriptomic data (Supplemental Figure 7A). This upregulation of the *TTL* genes in response to BR was confirmed at the cellular level by analyzing transgenic plants transformed with the reporter β-glucuronidase gene driven by each of the *TTL* promoters (Supplemental Figure 7B).

We next analyzed the sensitivity to epibrassinolide (eBL) by measuring root growth in the presence or absence of exogenous 100 nM eBL in wild-type Columbia ecotype (Col-0), single *ttl* mutants, the triple *ttl134* mutant, and *bak1-4*, a well-established mutant affected in BR responses (Chinchilla et al., 2007; He et al., 2007; Schwessinger et al., 2011; Gou et al., 2012). Single *ttl* mutants, the *ttl134* mutant, and the *bak1-4* mutant showed a similar root growth to Col-0 in control conditions (Figure 2A and Supplemental Figure 8A). However, *bak1-4*, *ttl1*, *ttl3*, and *ttl4* show increased root length compared with the Col-0 control or *ttl2* in the presence of eBL (Figure 2A and Supplemental Figure 8B). The lack of *ttl2* sensitivity to BR is consistent with the pollen-specific expression of *TTL2* (Lakhssassi et al., 2012). This decreased sensitivity to eBL of single *ttl* mutants was strongly enhanced in *ttl134* (Figure 2A and Supplemental Figure 8B). Root growth sensitivity to eBL of the *ttl134* mutant was then compared, in addition to *bak1-4*, to well-characterized genotypes affected in BR responses such as *serk1-1* and the double *serk1-1 bak1-4* mutant (Gou et al., 2012). In control conditions, all genotypes grew similar to Col-0, with the exception of *serk1-1 bak1-4*, which showed reduced root growth (Figure 2B and Supplemental Figure 8C), as reported previously (Du et al., 2012; van Esse et al., 2013). In the presence of 100 nM eBL, the root growth reduction of the Col-0 control was significantly higher than for the rest of the genotypes, including *ttl134* (Figure 2B; Supplemental Figure 8D), while the *serk1-1 bak1-4* double mutant was almost completely insensitive to eBL, as it showed a similar root growth in control and eBL-supplemented media.

Hypocotyl elongation in the dark is dependent on active BR signaling (Bernardo-García et al., 2014); therefore, it was analyzed in *ttl3*, *ttl134* and *bak1-4* as a readout of defective BR signaling (Zhang et al., 2015). As reported previously, *bak1-4* showed a reduction in hypocotyl elongation relative to Col-0 (Figure 2C; Supplemental Figure 8E; Li et al., 2002; Nam and Li, 2002). Similar to *bak1-4*, *ttl3* and *ttl134* mutants presented shorter hypocotyls than Col-0 (Figure 2C; Supplemental Figure 8E).

To investigate the contribution of *TTL* genes to BR responses at the molecular level, we first studied the expression of the BR-regulated genes *CPD1* and *DWF4* in Col-0, *bak1-4*, and the triple *ttl134* mutants. As shown in Figure 2D, *DWF4* and *CDP1* expression was approximately twofold higher in *ttl134* and *bak1-4* compared with the Col-0 control. This increased *CPD1* and *DWF4*

Figure 1. (continued).

(B) Schematic representation of BRI1 protein and the nine Ser/Thr residues of the JM and CT domains that were substituted by Asp in the BAK1-independent, BRI1-constitutive (phosphomimetic) active form BRI1cyt^{JMCT9D} (Wang et al., 2008). LRR, leucine rich repeat. Yellow-circled P's means that BRI1cyt^{JMCT9D} mimics the phosphorylated form of BRI1.

(C) Schematic representations of full-length and different truncated versions of TTL3 protein. Numbers indicate first and last amino acids (a.a.) of TTL3 truncated proteins. Domains and protein fragments interspacing the conserved domains are represented with the same color code as in **(A)**.

(D) TTL3ΔN1 interacts with BRI1cyt^{JMCT9D} in vitro, as shown by a GST-pull-down assay. GST-TTL3ΔN1 and GST-TTL3ΔN3 were detected with anti-GST antibody. MBP-BRI1cyt and MBP-BRI1cyt^{JMCT9D} were detected using specific anti-BRI1 antibodies (Bojar et al., 2014). Pull-down reflects 20% of the total pulled down proteins. Unbound reflects 1% of the total unbound fraction.

(E) BRI1-HA co-IPs with GFP-TTL3 full-length and GFP-TTL3 truncated versions ΔN1, ΔN2, and ΔC1. Numbers indicate first and last amino acids of TTL3 truncated proteins. BRI1-HA was transiently coexpressed in *N. benthamiana* with GFP-TTL3 full-length and truncated versions, and GFP-tagged protein was immunoprecipitated using anti–GFP-Trap beads. Total (input), IP, and CoIP proteins were analyzed by immunoblotting. Equal loading was confirmed by Coomassie blue staining (CBB) of input samples. GFP- and HA-tagged proteins were detected with anti-GFP and anti-HA antibody, respectively. The amount of coIP BRI1-HA was normalized relative to the amount of GFP-tagged protein from the input, dividing the signal intensity of coIP BRI1-HA by the signal intensity of the each GFP-tagged protein from the input that coIP BRI1-HA.

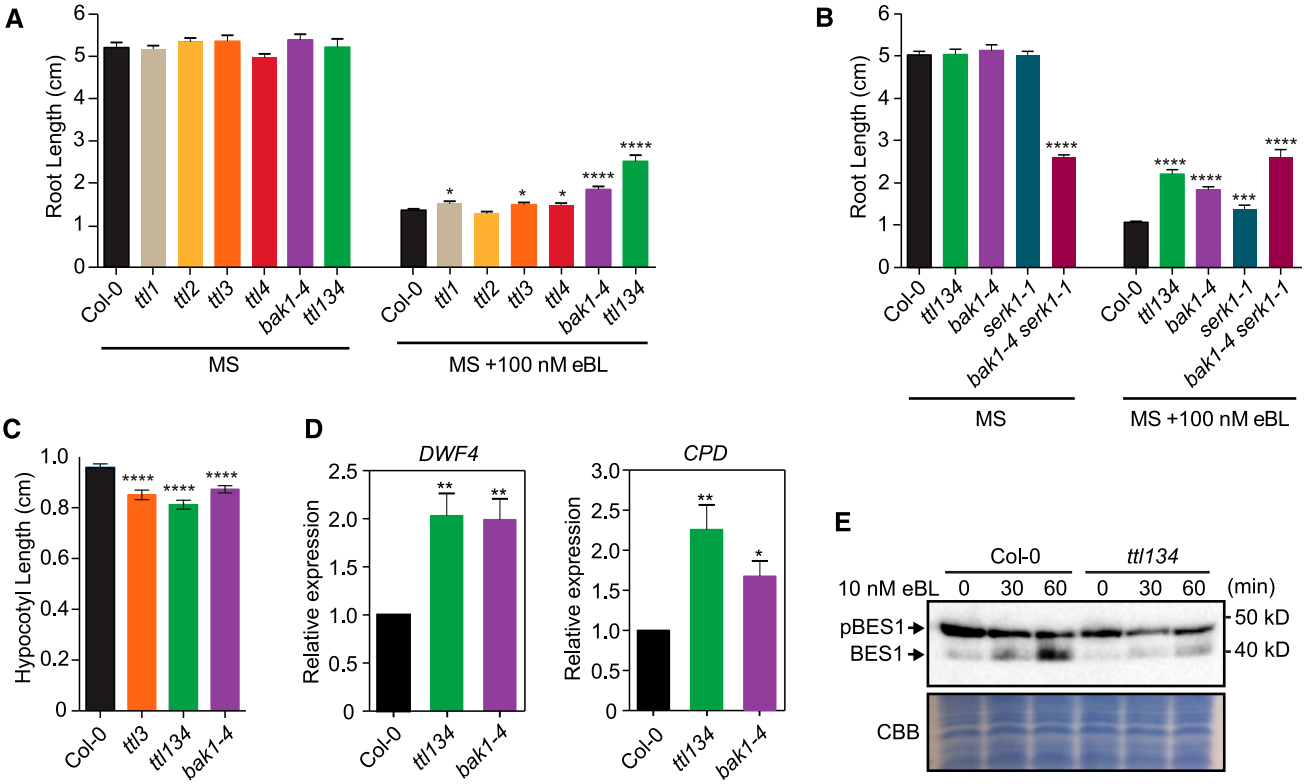

Figure 2. *TTL1*, *TTL3*, and *TTL4* Genes Play a Positive Role in BR Signaling.

(A) *ttl1*, *ttl3*, *ttl4*, and *ttl134* show root growth hyposensitivity to BR. Statistical analysis of root length measurements of Col-0, *ttl*, and *bak1-4* mutants in control conditions (MS) and in response to eBL. Seedlings were grown in long days for 4 d in half-strength MS agar solidified medium and then transferred to half-strength MS agar solidified medium (MS) or half-strength MS agar solidified medium supplemented with 100 nM eBL (MS + 100 nM eBL), and root length was measure 6 d later. Asterisks indicate statistical differences between mutant versus Col-0 determined by the unpaired *t* test (*P ≤ 0.05, **P ≤ 0.01, ***P ≤ 0.001 ****P ≤ 0.0001). Data represent mean values, error bars are SEM, $n \geq 35$ seedlings per experiment. The experiment was repeated three times with similar results.

(B) Root length responses to eBL of wild-type Col-0, *ttl134*, and BR perception mutants. Seedlings were grown and root length was analyzed as described in **(A)**. Asterisks indicate statistical differences between mutant versus Col-0 as determined by the unpaired *t* test (***P ≤ 0.001, ****P ≤ 0.0001). Data represent mean values, error bars are SEM, $n = 30$ seedlings per experiment. The experiment was repeated three times with similar results.

(C) Defective hypocotyl elongation in *ttl* mutants. Col-0, *ttl3*, *ttl134*, and *bak1-4* seedlings were grown for 4 d in long-day photoperiod in half-strength MS agar solidified medium. Seedlings with the same size were then placed in the dark, and hypocotyl elongation was measured 3 d later. Asterisks indicate statistically significant differences between Col-0 and the indicated genotype as determined by the unpaired *t* test (****P ≤ 0.0001), values are mean, error bars are SEM, $n = 80$ seedlings per experiment. The experiment was repeated twice with similar results.

(D) BR-responsive genes *DWF4* and *CPD* show induced expression in *ttl134* and *bak1-4* relative to Col-0 seedlings. Seeds were germinated in half-strength MS agar solidified medium and grown vertically in long-day photoperiod conditions. Five-day-old seedlings were transferred to half-strength MS liquid medium and after 5 d of acclimation, the relative expression level of *DWF4* and *CPD* was measured by RT-qPCR. The expression of *DWF4* and *CPD* was first normalized to the expression of *ACTIN2* and represented relative to the expression of Col-0. The data are shown as mean ± SEM from at least three independent biological replicates (pool of 20 seedlings per biological replicate). Asterisks indicate statistically significant differences between the indicated genotype versus Col-0 as determined by the unpaired *t* test (*P ≤ 0.05, **P ≤ 0.01). The experiment was repeated three times with similar results.

(E) Phosphorylation status of BES1 in response to exogenously applied eBL in Arabidopsis Col-0 and *ttl134*. Ten-day-old seedlings pre-treated for 3 d with the BR biosynthetic inhibitor BRZ to deplete the endogenous pool of BRs were subjected to 10 nM eBL treatment for 0, 30, and 60 min. Total proteins from a pool of 20 seedlings were analyzed by an immunoblot assay with a specific anti-BES1 antibody (Yu et al., 2011). The top band corresponds to pBES1 and the bottom band to dephosphorylated BES1 (BES1). The experiment was repeated two times with similar results. CBB, Coomassie blue.

expression has been reported for BR signaling mutants such as *bri1-5* (Wang et al., 2016), *bri1-301* (Gou et al., 2012), and *bik1* (Lin et al., 2013) and is caused by a lack of feedback regulation in the expression of these biosynthetic genes (Tanaka et al., 2005; Chung and Choe, 2013; Vriet et al., 2013). Second, we investigated the phosphorylation status of BES1 in Col-0 and the *ttl134* mutant in response to eBL. Because the BR biosynthetic genes *DWF4* and *CDP1* are already induced in *ttl134*, to fully capture the BR signaling capacity of *ttl134*, we pretreated the seedlings with the BR biosynthesis inhibitor BRZ. Without BR treatment, a strong signal of phosphorylated BES1 (pBES1) and a weak signal of dephosphorylated (BES1) are present in Col-0 and *ttl134*

(Figure 2E). While 10 nM eBL caused an increase of dephosphorylated BES1 in Col-0 after 30 and 60 min, eBL caused little dephosphorylation of pBES1 in *ttl134* seedlings (Figure 2E), confirming a defective BR signaling in *ttl134*.

Despite the role exerted by *TTL* genes in BR responses, *ttl134* adult plants do not exhibit obvious growth defects when under short-day or long-day photoperiod (Figure 3A and Supplemental Figure 9A). Phenotypic defects in BR sensitivity are often revealed in adult plants when mutations in potential BR signaling components are combined with weak *bri1* alleles (Nam and Li, 2002; Kim and Wang, 2010; Schwessinger et al., 2011). Therefore, we generated and analyzed the phenotype of a quadruple homozygous *ttl134 bri1-301* mutant. When grown in short days, the *bri1-301* mutant displays a semi-dwarf cabbage-like rosette, a phenotype that was enhanced in the *ttl134 bri1-301* quadruple mutant (Figure 3A). *ttl134 bri1-301* plants have fewer leaves than *bri1-301* plants (Supplemental Figure 9B), and the younger leaves were considerably smaller in *ttl134 bri1-301* than in *bri1-301* plants of the same age (Figure 3B). A stronger dwarf phenotype in *ttl134 bri1-301* relative to the weak *bri1-301* mutant was also observed in long-day-grown plants (Supplemental Figure 9A). *ttl134 bri1-301* also shows enhanced defects in seedling root growth (Figure 3C; Supplemental Figure 9C) and hypocotyl elongation (Figure 3D) relative to *bri1-301*. Next, we determined the root growth BR sensitivity of *ttl134 bri1-301* relative to Col-0, *ttl134*, and *bri1-301* (Ren et al., 2019). The *ttl134 bri1-301* seedlings exhibited less root growth inhibition than *bri1-301* seedlings when grown on 500 nM eBL (Figure 3E).

The gain-of-function *bes1-D* mutant shows constitutive BR responses, including higher elongation of hypocotyl and petioles due to increased levels of BES1 protein (Figures 3A and 3D; Yin et al., 2002). A *ttl134 bes-1D* quadruple mutant displays shorter hypocotyls and petioles than *bes1-D* (Figures 3A and 3D; Supplemental Figure 9D). This indicates that mutations in *TTL* genes reduce BR responses of *bes1-D*. Together, these results indicate that the TTLs play a positive role in the regulation of BR responses.

BRs Regulate the Cytoplasmic/Plasma Membrane Localization of TTL3

To further explore how TTL3 functions in BR signaling, we analyzed its subcellular localization. Although the BiFC interaction of

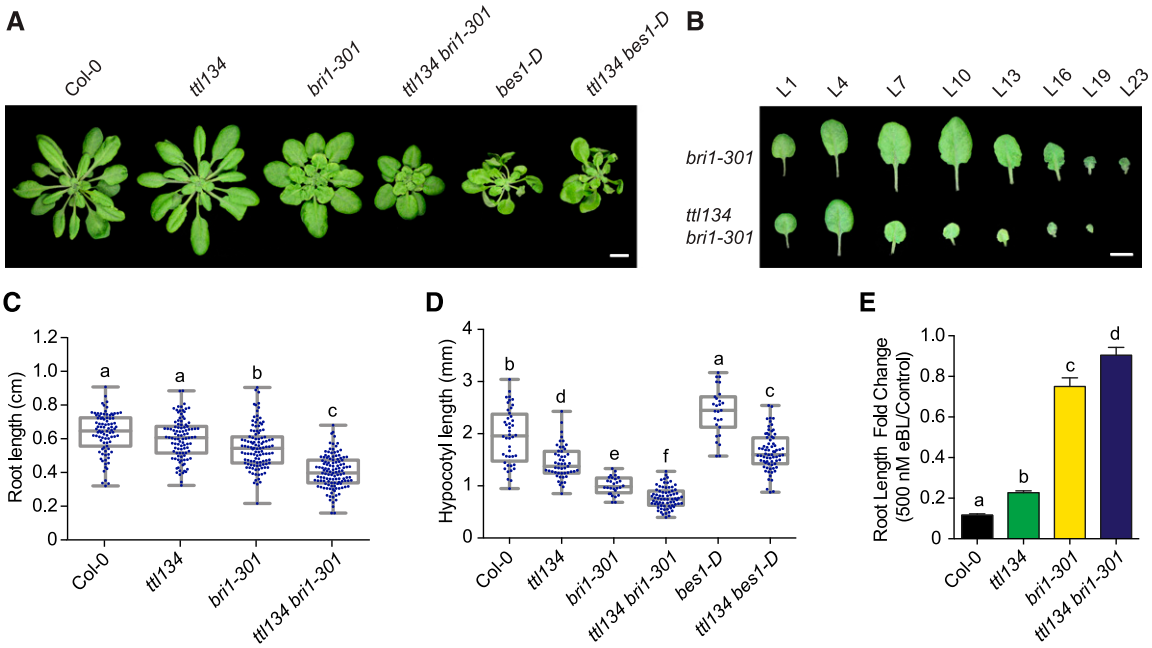

Figure 3. *ttl134* Mutations Enhance the *bri1-301*–Defective Phenotype and Partially Reduce the BR Responses in *bes1-D.*

(A) Morphological phenotypes of 5-week-old plants grown in short days. Bar = 1 cm.

(B) Detached leaves of 5-week-old plants grown in short days (L1, oldest leaf; L23 youngest leaf). Bar = 1 cm.

(C) Root length of 3-d-old seedlings grown in long days in half-strength MS agar solidified medium. Dots represent individual measurements from three independent experiments. *n* denotes measurement of roots from independent seedlings: Col-0 ($n = 92$), *ttl134* ($n = 100$), *bri1-301* ($n = 113$), and *ttl134 bri1-301* ($n = 123$). Box plots display the first and third quartiles, split by the median; whiskers extend to include the maximum and minimum values. Different lowercase letters indicate significant differences. Data were analyzed with one-way ANOVA and Tukey's multiple comparison test; $P < 0.05$.

(D) Hypocotyl length of 7-d-old seedlings grown in long days in half-strength MS agar solidified medium. Dots represent individual measurements from three independent experiments. *n* denotes measurement of hypocotyls from independent seedlings: Col-0 ($n = 44$), *ttl134* ($n = 51$), *bri1-301* ($n = 28$), *ttl134 bri1-301* ($n = 73$), *bes1-D* ($n = 27$), and *ttl134 bes1-D* ($n = 71$). Values are plotted and statistically analyzed as in **(C)**.

(E) Root length fold changes of seedlings grown for 7 d in the absence (control) or presence of 500 nM eBL in long days. Values are mean, error bars are SEM, and $n = 22$ seedlings per experiment. Different lowercase letters indicate significant differences. Data were analyzed with one-way ANOVA and Tukey's multiple comparison test; $P < 0.05$. The experiment was repeated twice with similar results.

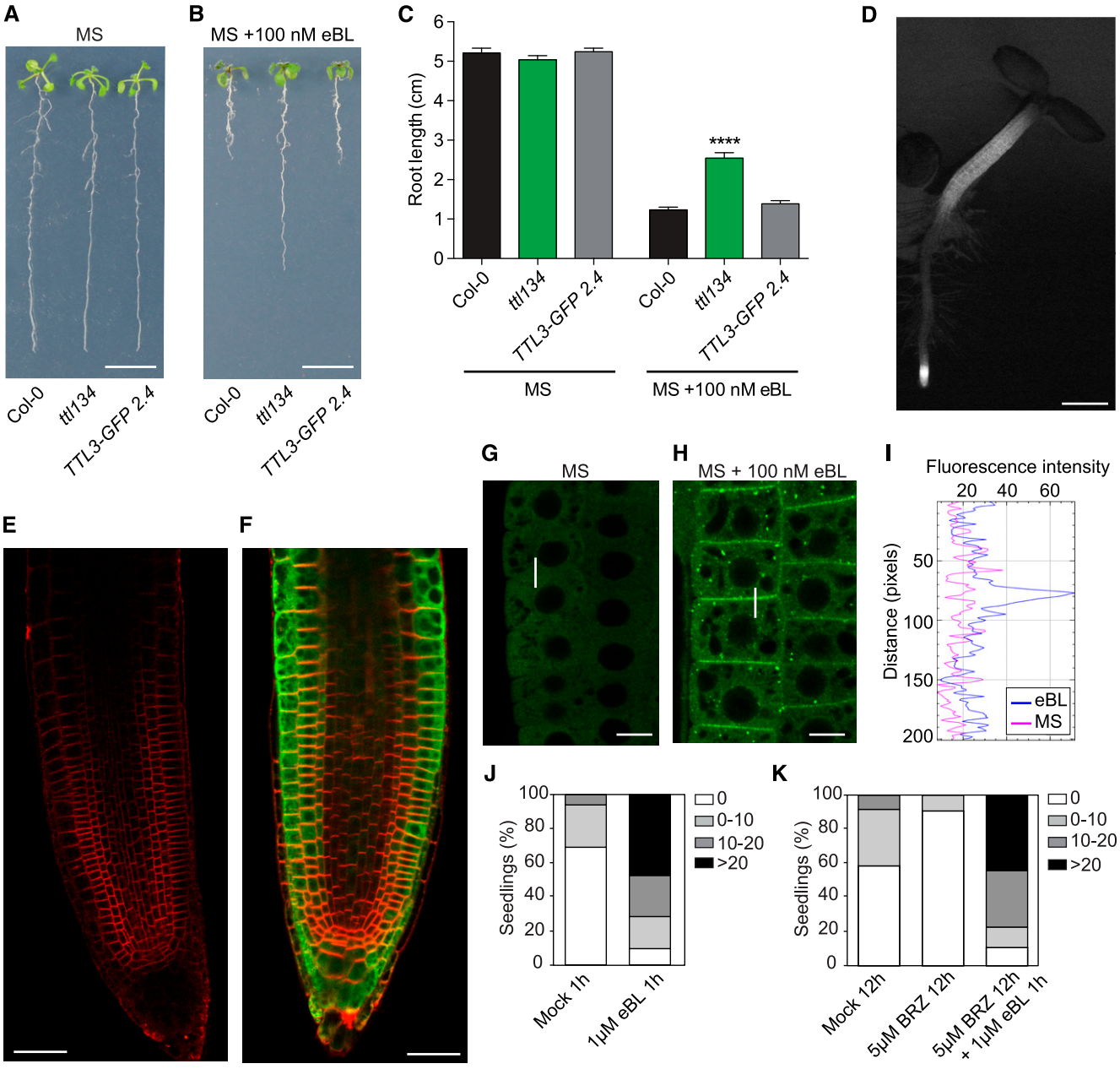

Figure 4. BRs Regulate the Cytoplasmic/Plasma Membrane Localization of TTL3.

(A) to **(C)** The root growth responses to eBL of the *ttl134* triple mutant are complemented in *TTL3-GFP 2.4*. Seedlings were grown for 4 d in half-strength MS agar solidified medium and then transferred to half-strength MS agar solidified medium **(A)** or half-strength MS agar solidified medium supplemented with 100 nM brassinolide **(B)** and root length was measured **(C)**. **(A)** and **(B)** Representative photographs of seedlings, 6 d after being transferred to control or eBL treatment. Bar in **(A)** and **(B)** = 1 cm. **(C)** Statistical analysis of root length of Col-0, *ttl134*, and the complementation line *TTL3-GFP* 2.4. Asterisks indicate statistically significant differences between the indicated genotype versus Col-0 as determined by the unpaired *t* test (****P ≤ 0.0001). Data represent mean values, error bars are SEM, and $n = 30$ seedlings per experiment. The experiment was repeated three times with similar results.

(D) Expression pattern of *TTL3-GFP* in 3-d-old *TTL3-GFP 2.4* Arabidopsis seedlings. Images were captured using conventional wide field fluorescence microscopy with a GFP filter. Bar = 500 μm.

(E) and **(F)** Longitudinal median section of root tips of a 3-d-old Col-0 **(E)** and *TTL3-GFP 2.4* seedling as observed by laser scanning confocal microscopy **(F)**. Images are a merge of green channel showing TTL3-GFP expression and red channel showing plasma membrane stained with FM4-64. Bar = 20 μm.

(G) and **(H)** Confocal images showing localization of TTL3-GFP in epidermal cells from the root meristematic zone in 4-d-old Arabidopsis *TTL3-GFP 2.4* in half-strength MS agar solidified medium, in control conditions (1-h treatment with eBL solvent) **(G)**, or after 1 h of 1 μM eBL treatment **(H)** in half-strength MS agar liquid medium. Bar = 10 μm (horizontal bar). **(I)** Quantification of fluorescent protein signal in plasma membrane versus cytoplasm. Line scan

TTL3 with BRI1 suggests a plasma membrane localization of TTL3, expression of a C-terminal GFP-tagged TTL3 in *N. benthamiana* indicated a predominant cytoplasmic localization in basal conditions (Supplemental Figure 10A). However, plasmolyzed cells show the presence of GFP-TTL3 in Hechtian strands, indicating that TTL3 also associated with the plasma membrane (Supplemental Figure 10B). To gain further insight into TTL3 localization, a genomic fragment including a 1.7-kb *TTL3* promoter region upstream of the start codon was transcriptionally fused to GFP to generate the *TTL3p*:*TTL3g-GFP* construct and transformed into both *ttl3* and *ttl134* mutants using *Agrobacterium tumefaciens*. After confocal analysis of a large number of independent stable transgenic lines, we selected two homozygous lines, one in the *ttl3* background (hereafter *TTL3-GFP 1.2*) and the other in the *ttl134* background (*TTL3-GFP 2.4*), which presented noticeable fluorescence signals. Venation defects of *ttl3* and *ttl134* were restored to levels similar to Col-0 in *TTL3-GFP 1.2* and *TTL3-GFP 2.4* (Supplemental Figure 1B). Furthermore, root growth of *TTL3-GFP 1.2* (Supplemental Figures 11A and 11B) and *TTL3-GFP 2.4* (Figures 4A to 4C) were restored to wild-type levels in the presence of eBL, indicative of a functional TTL3-GFP protein.

We then used *TTL3-GFP 2.4* (which showed a stronger fluorescence signal than *TTL3-GFP 1.2*) to analyze the cellular and subcellular localization of TTL3. Examination under a stereomicroscope indicated that TTL3-GFP accumulated mainly at the root tip and the hypocotyl of Arabidopsis seedlings (Figure 4D). This accumulation coincides with cells that undergo strong BR signaling, leading to active growth, and highly resembles the accumulation pattern of BRI1-GFP (Geldner et al., 2007; Wilma van Esse et al., 2011; Fàbregas et al., 2013). Cellular analysis using confocal microscopy was performed in 3-day-old roots, simultaneously localizing TTL3-GFP with the FM4-64, a lipophilic red dye that labels the plasma membrane and tracks plasma membrane-derived endosomes (Vida and Emr, 1995). In Col-0 control roots, no GFP signal was detected (Figure 4E), while analysis of *TTL3-GFP 2.4* revealed the presence of TTL3-GFP in all cell files of the root apical meristem (Figure 4F). Further up, in the meristematic region, TTL3-GFP showed a predominant localization in the outer cell layers (epidermis and cortex; Figure 4F).

At the subcellular level, TTL3-GFP mostly showed a cytoplasmic localization in the root meristematic cells (Figure 4G). However, we sometimes observed seedlings that, in addition to the cytoplasmic GFP localization, showed GFP signal at the plasma membrane. Quantification of the plasma membrane localization of TTL3-GFP (see Figure 4G legend and "Methods" for details) in control growth conditions indicated that in ~30% of the seedlings some cells showed TTL3-GFP localization at the plasma membrane (Figure 4J). Treatment with 1 μM eBL, a concentration previously used to analyze short-term BRI1 KINASE INHIBITOR1 dynamics (Wang and Chory, 2006), increased the amount of TTL3-GFP protein (Supplemental Figures 12A and 12B) consistent with the increased expression of *TTL3* by BRs. Interestingly, exogenous eBL treatment enhanced the relocalization of TTL3-GFP from the cytoplasm to the plasma membrane (Figures 4H to 4J; Supplemental Figures 13A and 13B). eBL treatment also caused the appearance of GFP-labeled intracellular structures (Figure 4H). These intracellular TTL3-GFP structures do not colocalize with FM4-64 (Supplemental Figure 13A), eliminating the possibility that they correspond to plasma membrane–derived endosomes; thus, their identity remains elusive.

Consistent with the possibility that the plasma membrane localization of TTL3-GFP in seedlings grown in control medium was caused by endogenous BRs, the percentage of seedlings with plasma membrane signal decreased from ~30 to ~5% after treatment with BRZ (Figure 4K). Further treatment of these seedlings with eBL reverted this effect and increased the plasma membrane localization of TTL3-GFP (Figure 4K).

TTL3 Associates with the BR Signaling Components BSK1, BSU1, and BIN2 and Directly Interacts with BSU1

Our previous analyses indicate that TTL proteins are required for BR signaling. Considering the structure of these proteins and the interaction of TTL3 with BRI1, one possibility is that these TTL proteins function as a scaffold of additional BR signaling components. We first investigated possible direct interactions between TTL3 and the cytoplasmic BR signaling components BSK1, BSU1, and BIN2, using yeast two-hybrid assays. Using a full-length TTL3 protein, we did not identify interactions with any of the investigated BR components (Figure 5A). However, immunoblot analysis indicated that BD-TTL3 fusion protein was not produced (Supplemental Figure 14), similar to what previously occurred in *E. coli*. Therefore, we generated additional yeast two-hybrid constructs using the TTL3ΔN1 and TTL3ΔN2 fragments (Figure 1C). As shown in Figure 5A, TTL3ΔN1, but not TTL3ΔN2, interacted with BSU1, indicating that the six TPR domains are required for the interaction. In contrast to BSU1, BIN2 and BSK1 did not interact with TTL3ΔN1 (Figure 5A). As a control, we used the positive interaction of BIN2 with BSU1 as described previously (Kim et al., 2009).

Figure 4. (continued).

measurements spanning membrane and cytoplasm were performed (represented in **[G]** and **[H]** as a vertical white line), and representative plot profiles of sample measurements are presented.

(J) and **(K)** Quantification of the cytoplasmic and plasma membrane localization of TTL3-GFP in 4-d-old Arabidopsis *TTL3-GFP 2.4* seedlings treated for 1 h with 1 μM eBL **(J)** or pre-treated for 12 h with 5 μM BRZ prior to 1 μM eBL application for 1 h **(K)**. The number of cells with dual cytoplasmic/plasma membrane localization in meristematic and transition zone was counted for each analyzed root using confocal microscopy. Seedlings were grouped in categories according to the number of cells that presented this dual localization, and the percentage of seedlings displaying each category depicted in the key was calculated. Represented categories in the key indicate the number of cells per seedling with dual cytoplasmic/plasma membrane localization. At least 16 seedlings per treatment, and ~200 cells (cell from epidermis, cortex, and endodermis all combined) per seedling of the meristematic region of the root tip were analyzed.

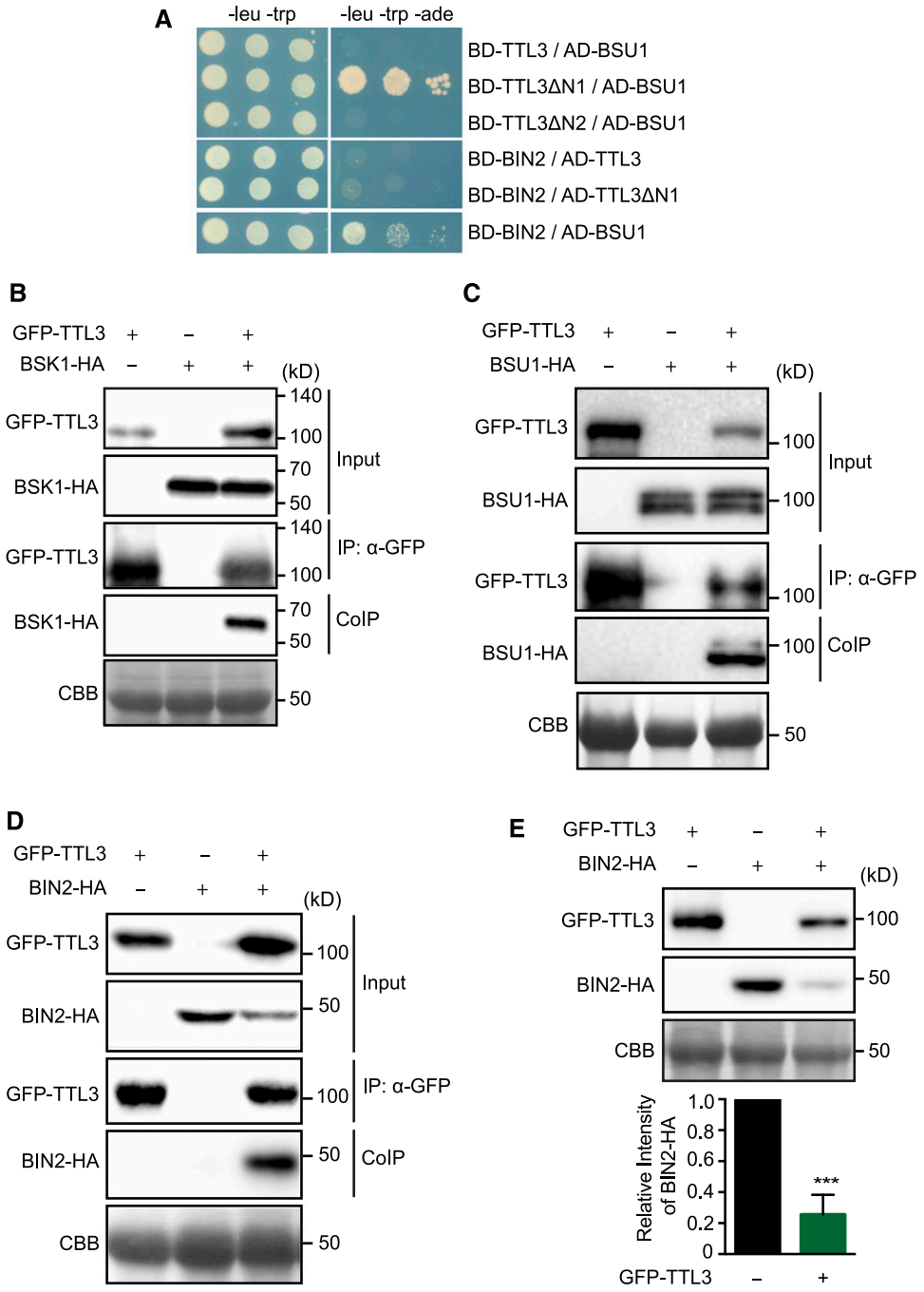

Figure 5. TTL3 Associates with BSK1 and BIN2 and Directly Interacts with BSU1.

(A) Yeast-two-hybrid assays to determine the interaction of full-length TTL3, the TTL3 fragment TTL3ΔN1 (amino acids 204 to 691), and the TTL3 fragment TTL3ΔN2 (amino acids 371 to 691) with BIN2 and BSU1. Growth on plasmid-selective media (left column) and interaction-selective media (lacking adenine [-ade], right column) are shown.

(B) BSK1 co-immunoprecipitates with TTL3. BSK1-HA, and GFP-TTL3 were transiently expressed in *N. benthamiana*. GFP-TTL3 was IP with anti-GFP Trap beads. Total (input), IP, and CoIP proteins were analyzed by immunoblotting. Equal loading was confirmed by Coomassie blue staining (CBB) of input samples. GFP-TTL3 and BSK1-HA were detected with anti-GFP and anti-HA antibody, respectively.

(C) BSU1 co-immunoprecipitates with TTL3. GFP-TTL3 and BSU-HA proteins were transiently expressed in *N. benthamiana*, IP, and analyzed as described in **(B)**. GFP-TTL3 and BSU1-HA were detected with anti-GFP and anti-HA antibodies, respectively.

(D) BIN2 co-immunoprecipitates with TTL3. BIN2-HA and GFP-TTL3 proteins were expressed in *N. benthamiana*, IP, and analyzed as described in **(B)**. GFP-TTL3 and BSU1-HA were detected with anti-GFP and anti-HA, respectively.

Next, we used Co-IP and BiFC in *N. benthamiana* to investigate possible associations of TTL3 with BSK1, BSU1, and BIN2. TTL3 strongly associates with BSK1 in both Co-IP (Figure 5B) and BiFC assays (Supplemental Figure 6A). BiFC between TTL3 and BSK1 was also obtained when we exchanged nYFP and cYFP tags (Supplemental Figure 6B) and, consistent with the plasma membrane localization of BSK1, the BiFC signal for BSK1-TTL3 was observed at the plasma membrane. TTL3 also associated with BSU1 and BIN2 in both Co-IP and BiFC assays (Figures 5C and 5D; Supplemental Figures 6A and 6B). Although BSU1 and BIN2 present a dual nuclear and cytoplasmic localization (Vert and Chory, 2006; Maselli et al., 2014), BiFC signals were only observed in the cytoplasm for both TTL3-BSU1 and TTL3-BIN2, which is consistent with the lack of TTL3 protein in the nucleus. A cytoplasmic BiFC signal was also obtained when YFP halves were interchanged among TTL3-BSU1 and TTL3-BIN2 (Supplemental Figure 2B). Interestingly, we consistently observed that when TTL3 was coexpressed with BIN2, there was a depletion of BIN2 protein amount in the total protein extract (Figure 5D, input). This was further quantified using six biological replicates, confirming that upon TTL3 expression the levels of BIN2 were reduced by ~80% (Figure 5E). This was unique for BIN2 since we did not find the same effect with any other protein of the BR pathway (Figures 1E, 5B, and 5C) and suggests that TTL3 might function, at least in part, in BR signaling, by negatively regulating the amount of BIN2.

TTL3 Interacts with the Transcription Factors BZR1 and Affects Its Cytoplasmic/Nuclear Localization

In the absence of BRs, BIN2 phosphorylates and inactivates BZR1 and BES1, the two major transcription factors mediating BR-induced transcriptional changes (Belkhadir and Jaillais, 2015). We performed a yeast two-hybrid assay between TTL3 and the transcription factor BZR1 (Figure 6A). As a positive control (Figure 6A), we used the reported interaction between BZR1 with BIN2 (He et al., 2002). As expected, based on the lack of accumulation of the full-length TTL3 protein in yeast (Supplemental Figure 14), no interaction with BZR1 was obtained (Figure 6A). However, we did detect an interaction between TTL3ΔN1 and TTL3ΔN2 (Figure 1C) and BZR1 (Figure 6A), indicating that the TPR3-to-TPR6 region of TTL3 is sufficient for its interaction with BZR1.

TTL3 also associates with BZR1 in Co-IP experiments in *N. benthamiana* (Figure 6B) and in Arabidopsis mesophyll protoplasts (Figure 6C). Phosphorylated and dephosphorylated BZR1 proteins show a marked difference in mobility in SDS-PAGE upon expression in *N. benthamiana* (Figure 6B; Supplemental Figure 15A) and in Arabidopsis protoplasts (Figure 6C; Gampala et al., 2007; Ryu et al., 2007). Interestingly, only the pBZR1 was CoIP with TTL3 (Figure 6C; Supplemental Figure 15A), suggesting a preferential association of TTL3 with pBZR1. BiFC assays further confirmed the in vivo association of BZR1 with TTL3 (Supplemental Figures 6A and 6B). We also observed that while the BiFC signal of TTL3 with plasma membrane BR components results in a smooth YFP fluorescence signal, the BiFC signal of TTL3 with the cytoplasmic components appears punctate (Supplemental Figures 6A and 6B). A similar punctate BiFC signal has been reported previously for BZR1 with BRZ-SENSITIVE-SHORT HYPOCOTYL1 (Shimada et al., 2015) or BES1 with DOMINANT SUPPRESSOR OF KAR2 (Nolan et al., 2017), although its significance remains unknown.

We then analyzed the effect of TTL3 on the nuclear and cytoplasmic localization of BZR1-GFP. As reported previously, BZR1-GFP in *N. benthamiana* is mainly localized in the nucleus (Figure 6D), while coexpression of BIN2 together with BZR1-GFP promotes its phosphorylation and its cytoplasmic retention (Figure 6D; Kim et al., 2009). Coexpressing TTL3-HA with BZR1-GFP and BIN2-HA suppressed the cytoplasmic retention of BZR1-GFP promoted by BIN2 (Figure 6D). We also used Arabidopsis plants expressing the salicylate hydroxylase (*NahG*) gene, as these plants are efficiently transiently transformed using *A. tumefaciens* (Rosas-Díaz et al., 2016). Similar to *N. benthamiana*, coexpressing BIN2-HA together with BZR1-GFP increased its cytoplasmic accumulation, which was further abolished by TTL3-HA (Supplemental Figure 15B). This BZR1 nuclear/cytoplasmic localization is associated with the dephosphorylation status of BZR1 (Figure 6E), indicating that TTL3 negatively regulates BIN2 phosphorylation of BZR1 and regulates its activity, likely by promoting BIN2 depletion (Figure 5E).

TTL3 Reinforces BSK1-BZR1 Association at the Plasma Membrane

The search for BZR1 interacting proteins in Arabidopsis through tandem affinity purification allowed the identification of BSK1 as a BZR1 interactor (Wang et al., 2013), a result that we confirmed using Co-IP (Supplemental Figure 16). This led the authors to suggest that BR signaling components exist in a multiprotein complex at the plasma membrane. The formation of a multiprotein complex for BR components at the plasma membrane has been recently proposed, with BSK3 (a protein that contain TPR domains) acting as a possible scaffold (Ren et al., 2019). Therefore, we aimed to investigate whether TTL3 could function as an additional scaffold in BR signaling. For this, we determined whether TTL3 expression affects the association at the plasma membrane of BSK1 with cytoplasmic BR components using BiFC. As shown in Figure 7A, a strong BiFC signal was obtained for BSK1 with BRI1, BSU1, and BIN2, while a weak signal was obtained with BZR1. The strong BiFC signal detected for BSK1 with BRI1 and with BSU1 is expected, since these BR signaling components

Figure 5. (continued).

(E) TTL3 promotes BIN2 depletion. BIN2-HA with and without GFP-TTL3 was expressed in *N. benthamiana*. Protein extracts were analyzed by immunoblotting. Equal loading was confirmed by Coomassie blue staining (CBB) of input samples. GFP-TTL3 and BIN2-HA were detected with anti-GFP and anti-HA antibody, respectively. Bottom graph represents the signal density of BIN2-HA coexpressed with or without GFP-TTL3 in *N. benthamiana* was quantified based on the six biological repeats. The immunoblot signal intensity of BIN2-HA coexpressed with GFP-TTL3 was normalized to the immunoblot signal intensity of BIN2-HA coexpressed with an empty vector. Asterisks indicate statistical differences as determined by the unpaired *t* test (***$P \leq 0.001$).

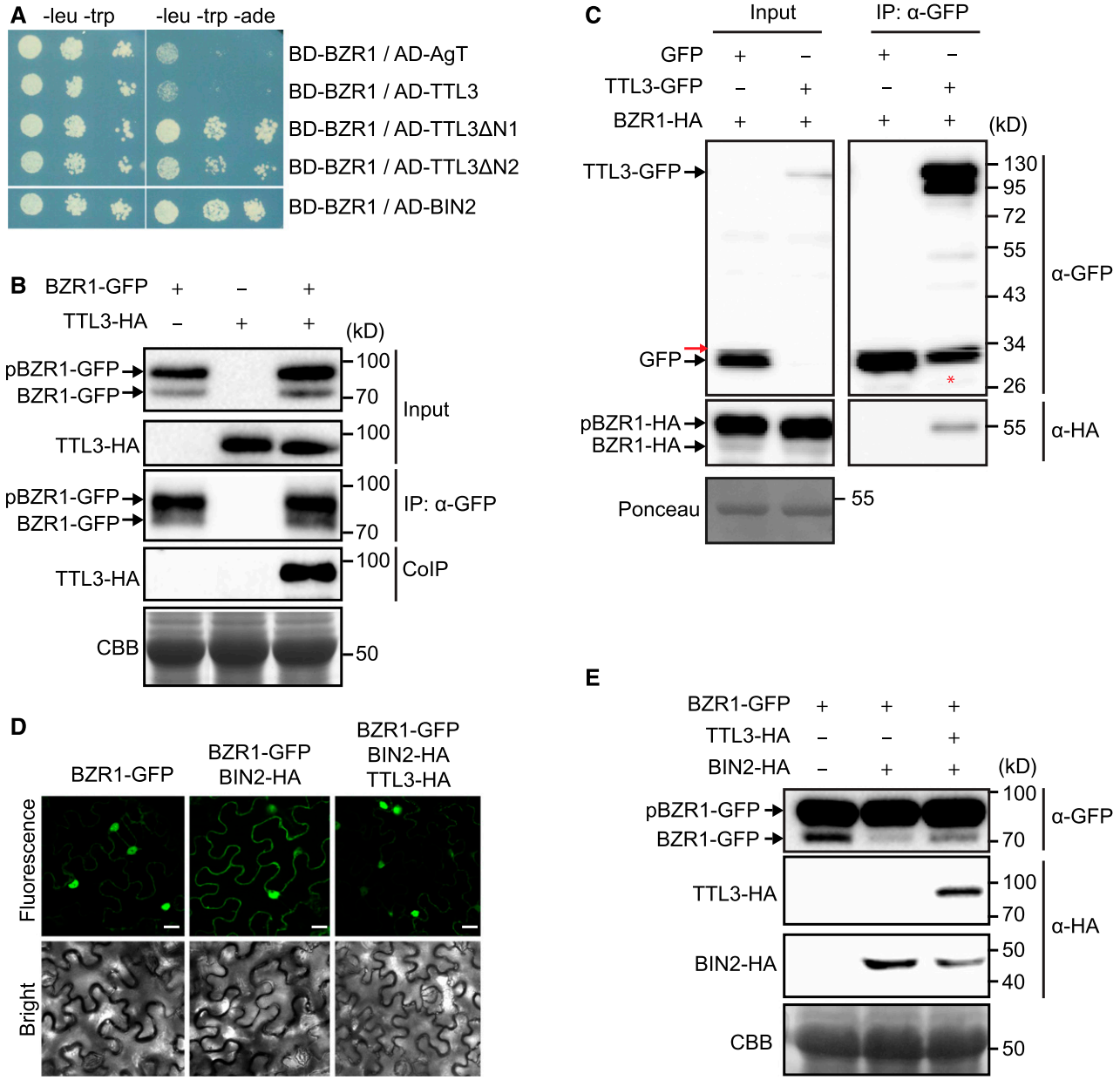

Figure 6. TTL3 Interacts with BZR1 and Regulates Its Cytoplasmic/Nuclear Localization.

(A) Yeast-two-hybrid assays to determine the interaction of BZR1 with TTL3, the TTL3 fragment TTL3ΔN1 (amino acids 204 to 691), the TTL3 fragment TTL3ΔN2 (amino acids 371 to 691), and BIN2. Interaction of BZR1 with a fragment of Simian virus 40 large T-antigen (AD-AgT) was also included to show BD-BZR1 self-activation capacity. Growth on plasmid-selective media (left column) and interaction-selective media (lacking adenine, -ade], right column) are shown.

(B) TTL3 co-immunoprecipitates with BZR1. TTL3-HA and BZR1-GFP were transiently expressed in *N. benthamiana*. BZR1-GFP was IP with anti-GFP Trap beads. Total (input), IP, and CoIP proteins were analyzed by immunoblotting. Equal loading was confirmed by Coomassie blue staining (CBB) of input samples. BZR1-GFP and TTL3-HA were detected with anti-GFP and anti-HA, respectively. The top band corresponds to phosphorylated BZR1 (pBZR1-GFP) and the bottom band to dephosphorylated BZR1 (BZR1-GFP).

(C) Co-IP of BZR1-HA with TTL3-GFP expressed in transfected Arabidopsis Col-0 protoplasts. Samples were analyzed as in **(B)**. Protoplasts cotransfected with free GFP and BRI1-HA, were used as a negative control for Co-IP. Equal loading was confirmed by Ponceau staining of input samples. TTL3-GFP and free GFP were detected with anti-GFP antibody and BRI1-HA was detected with anti-HA antibody. Asterisk indicates GFP that results from proteolytic cleavage of TTL3-GFP. Red arrow indicates an artifact from imaging the blot with high sensitivity using an Azure c300 Chemiluminescent Western Blot Imaging System.

directly interact with BSK1 (Kim et al., 2009). BIN2, although mainly localizing at the nucleus and cytosol, also localizes at the plasma membrane (Vert and Chory, 2006) and directly interacts with several plasma membrane–localized BSKs (Sreeramulu et al., 2013; Ren et al., 2019). Importantly, the BSK1-BZR1 BiFC signal was strongly enhanced when we coexpressed with TTL3-HA (Figures 7B and 7C), indicating that TTL3 increases the association between BSK1 and BZR1 at the plasma membrane. Further immunoblot analysis confirmed that the increase in BSK1-BZR1 BiFC fluorescence was not due to a differential expression of the BiFC proteins caused by TTL3 expression (Figure 7D).

DISCUSSION

The expression of *TTL* genes is induced by BRs and TTL3 shows its highest expression at the root elongation zone and at the hypocotyl, areas of high BR activity (González-García et al., 2011; Bernardo-García et al., 2014). Individual *ttl1*, *ttl3*, and *ttl4*, and particularly the triple *ttl134* mutants, are hyposensitive to BR in root growth assays and show reduced hypocotyl elongation. Further lines of genetic evidence supporting the function of *TTL* genes in BR signaling come from phenotypic analyses of the quadruple mutants of *ttl* genes with either *bri1-301* or *bes1-D*. At the molecular level, *ttl134* shows increased expression of BR-repressed genes, whereas BR-induced dephosphorylation of the transcription factor BES1 is strongly reduced. At the cellular level, a functional TTL3-GFP shows a dual localization in the cytoplasm and plasma membrane in untreated seedlings. Treatment with eBL caused TTL3-GFP relocalization from the cytoplasm to the plasma membrane, while treatment with a BR biosynthesis inhibitor had the opposite effect. Furthermore, coexpression of TTL3 together with BZR1 and BIN2 abolishes the BIN2-dependent BZR1 cytoplasmic retention in Arabidopsis and *N. benthamiana* (Gampala et al., 2007; Ryu et al., 2007; Kim et al., 2009; Tang et al., 2011). Overall, this study reveals that plant-specific TTL proteins function as positive regulators of BR signaling.

TTL proteins contain several defined domains involved in protein–protein interactions and assembly of multiprotein complexes. Consistent with this structure, TTL3 protein associates in vivo with all core BR signaling components, with the exception of BAK1, and interacts directly with BRI1, BSU1, and BZR1. Mapping the interaction domains of TTL3 with BRI1 indicates that the last four TPRs are essential for this interaction and that both TRLX and the IDR contribute to strengthen the interaction. The presence of an IDR in TTL proteins can provide additional advantages in their scaffolding and regulatory function since IDRs allow their interaction with a large number of partners due to their ability to adopt different conformations, thus allowing the assembly of multiple proteins (Soutourina, 2018). We also found that interaction of TTL3 with BSU1 requires all six TPRs, while only the last four TPR domains are required for the interaction with BZR1.

How does TTL function mechanistically in BR signaling? The BR-dependent plasma membrane relocalization of TTL3, probably through interaction with phosphorylated BRI1 and the association with other BR components, suggests that these proteins function as a scaffold by bringing them together at the plasma membrane. This is supported by the finding that a weak BZR1 and BSK1 association at the plasma membrane is greatly enhanced by TTL3 overexpression. Our data indicate that TTL3 promotes dephosphorylation and nuclear localization of BZR1, while TTL3 increased BiFC interaction of BSK1-BZR1 at the plasma membrane. These seemingly contradictory results can be explained by the irreversible assembly of the two YFP halves, an intrinsic feature of BiFC. It is possible that the stability of the BiFC complex formed between BSK1 and BZR1 facilitates the visualization of this likely transient interaction but will also hinder the dynamics of this protein complex formation (Kudla and Bock, 2016).

Although in current models of BR signaling phosphorylation/dephosphorylation of transcription factors take place exclusively in the cytoplasm and the nucleus (Wang et al., 2012; Belkhadir and Jaillais, 2015), a survey of the literature provides evidence that the plasma membrane could be an active site of BR signaling, from perception of the hormone to dephosphorylation of the transcription factors: (1) A significant amount of phosphorylated BZR1 located at the plasma membrane is greatly reduced upon BR treatment (Gampala et al., 2007). (2) BSK1 has been identified as an interactor of BZR1 using nontargeted proteomics, which led the authors to propose that BR signaling components exist in the plasma membrane as a multiprotein complex (Wang et al., 2013). (3) Several BSKs that are plasma membrane bound interact with BIN2, suggesting that dephosphorylation of BZR1 and BIN2 is also taking place at the plasma membrane (Sreeramulu et al., 2013; Maselli et al., 2014). In a recent report, BSK3 has been shown to directly interact with BRI1, BSU1, and BIN2 (Ren et al., 2019) and is proposed to function as a scaffold that positively regulates BR signaling by locating BSU1 and BIN2 at the plasma membrane and enhancing their interaction.

The basic function of scaffolding proteins is the assembly of signaling components that enhance the efficiency of the signaling cascade by increasing their local concentrations as well as the localization of the signaling reaction to a specific area of the cell. This could be particularly important in BR signal components because some of these proteins are expressed at vanishingly low levels, like BSU1 and BIN2 (Mora-García et al., 2004; Peng et al.,

Figure 6. (continued).

(D) TTL3 abolishes the cytoplasmic retention of BZR1 by BIN2. Subcellular localization of BZR1-GFP alone, coexpressed with BIN2-HA, and with BIN2-HA and TTL3-HA in *N. benthamiana* leaves. Images of the GFP signal were obtained using laser scanning confocal microscopy. Images show a single equatorial plane in *N. benthamiana* leaves. Bar = 20 μm. The experiment was repeated three times with similar results.

(E) Immunoblot analysis of the BZR1-GFP proteins transiently expressed alone, coexpressed with BIN2-HA, and coexpressed with BIN2-HA and TTL3-HA in *N. benthamiana* leaves observed by confocal microscopy in **(D)**. Proteins were analyzed by immunoblotting. Equal loading was confirmed by Coomassie blue staining (CBB) of input samples. BZR1-GFP was detected with anti-GFP antibody, while TTL3-HA and BIN2-HA were detected with anti-HA antibody. In the anti-GFP blot, the top band corresponds to phosphorylated BZR1 (pBZR1-GFP) and the bottom band to dephosphorylated BZR1 (BZR1-GFP).

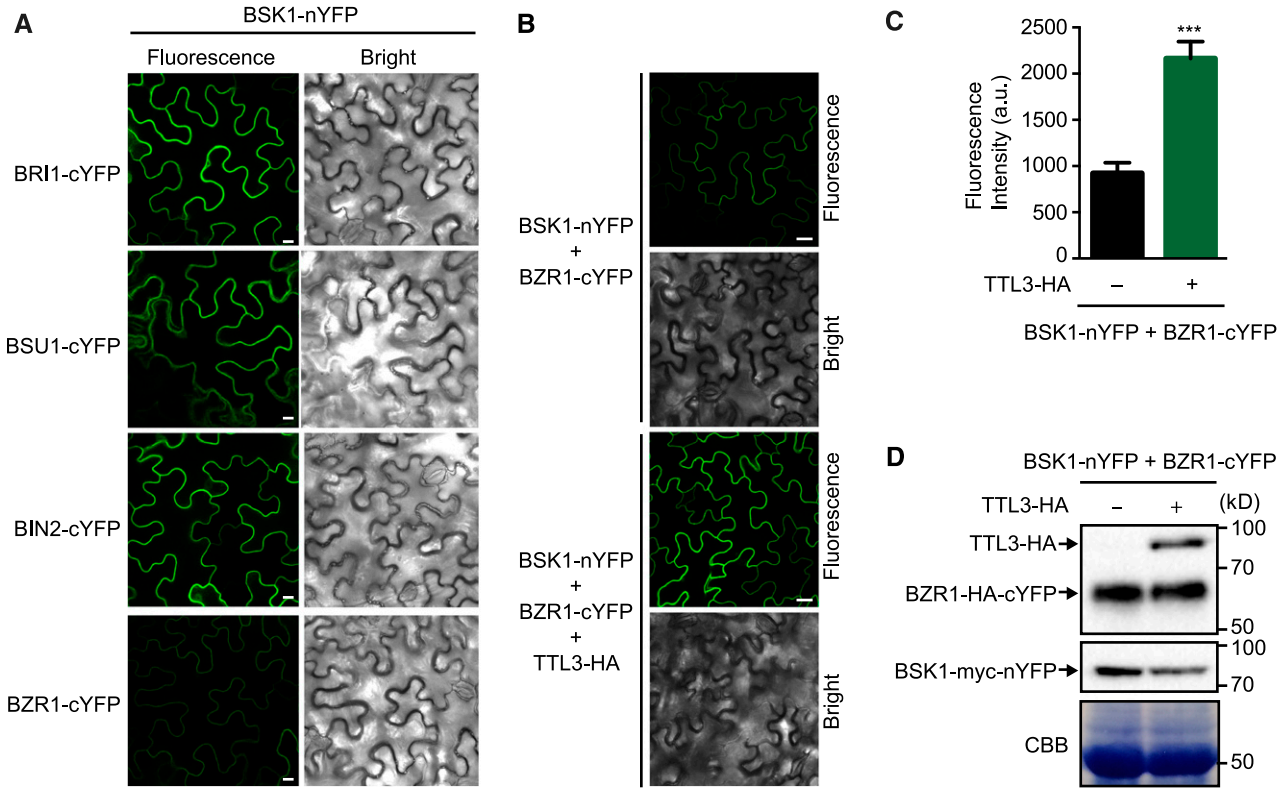

Figure 7. Coexpression of TTL3 Enhances pBZR1-BSK1 Interaction.

(A) BiFC shows strong association of BSK1 with BRI1, BSU1, and BIN2 and weak association with BZR1. *N. benthamiana* leaves were co-agroinfiltrated with the *Agrobacterium* strains harboring a construct to express the BSK1 protein fused to the N-terminal half of YFP and the BRI1, BSU1, BIN2, or BZR1 proteins fused to the C-terminal half of YFP and observed under a laser scanning confocal microscope. Strong fluorescence signals are observed when BSK1-nYFP is coexpressed with BRI1-cYFP, BSU1-cYFP, or BIN2-cYFP. A faint YFP signal is observed when BSK1-nYFP is coexpressed with BZR1-cYFP. From left to right columns, images show BiFC YFP fluorescence in green and bright-field. Bar = 20 μm. The experiment was repeated two times with similar results.
(B) Expression of TTL3 increases the weak BiFC association of BSK1 and BZR1. *N. benthamiana* leaves were co-agroinfiltrated with the *Agrobacterium* strains harboring the corresponding constructs to express the BSK1 protein fused to the N-terminal half of YFP and the BZR1 protein fused to the C-terminal half of YFP. *N. benthamiana* leaves were pre-treated with 5 μM eBL for 3 h before confocal imaging analysis. Coexpression of TTL3-HA together with BSK1-nYFP and BZR1-cYFP highly enhances the GFP signal. From left to right columns, BiFC YFP fluorescence in green and bright field. Bar = 20 μm. The experiment was repeated three times with similar results.
(C) Quantification of the BiFC fluorescence intensity of BSK1 and BZR1 in the presence or absence of TTL3-HA described in **(B)**. Asterisks indicate statistical differences between BiFC fluorescence intensity of BSK1 and BZR1 in the absence or presence of TTL3-HA determined by the unpaired *t* test (***$P \leq 0.001$). Data represent mean values, error bars are SEM, and $n = 5$ randomly chosen regions of infiltrated leaves. The experiment was repeated three times with similar results. a.u., arbitrary units.
(D) Immunoblot analysis reveals similar amounts of BSK1-nYFP and BZR1-cYFP when coexpressed with or without TTL3-HA. Proteins were transiently expressed as described in **(B)**. Equal loading was confirmed by Coomassie blue staining (CBB) of total proteins. BSK1-nYFP contains a myc tag (BSK1-myc-nYFP) and was detected using anti-myc antibody, while BZR1-cYFP contains a HA tag (BZR1-HA-cYFP) and was detected using an anti-HA antibody. TTL3-HA was also detected with an anti-HA antibody. The experiment was repeated three times with similar results.

2008). This scaffolding function of TTL proteins might also have a role in enhancing signaling specificity by preventing spurious interactions of BR signaling components. This is important because some BR signaling components participate in pathways other than BR. For example, BAK1 and related SERK coreceptors are involved in numerous responses (Ma et al., 2016) in addition to their role in BR signaling, and BIN2 shows multiple targets that result in different signaling outcomes (Kim et al., 2012; Cai et al., 2014). The importance of scaffold proteins to generate signaling specificity of BIN2 (and related GSK3-line kinases) was recently highlighted by the identification of the plant-specific protein POLAR (Houbaert et al., 2018). POLAR acts in concert with BREAKING OF ASYMMETRY IN THE STOMATAL LINEAGE as a stomatal lineage scaffold for GSK3-like kinases that confines them to specific subcellular localizations during stomatal differentiation (Houbaert et al., 2018). Another example is BSK1, originally identified in BR signaling by proteomic studies (Tang et al., 2008) but later found also to regulate immunity (Shi et al., 2013). Because *TTL1*, *TTL3*, and *TTL4* were previously reported to play a role in abiotic stress tolerance and there is increasing evidence for the coordination of BR-promoted growth and

abiotic stress responses (Zhang et al., 2016; Nolan et al., 2017; Tian et al., 2018), we cannot exclude that the function of TTL3 (and probably other TTLs) as a scaffold of BR signaling components contribute to this crosstalk.

Our work uncovers TTL proteins as components of BR signaling and places the BR pathway in a spatial context. BSK3 kinase has been show to function in early BR signaling by acting as a scaffold at the plasma membrane that mediates the assembly of BR components (Ren et al., 2019). Further characterization of these scaffold proteins will reveal how components of the BR cascade are spatially assembled so that their localization and local concentration are controlled for optimal signaling.

METHODS

Plant Material

All Arabidopsis (*Arabidopsis thaliana*) plants generated in this study are of the Col-0 ecotype. Arabidopsis mutants lines used in this study have been described previously: *ttl1* (AT1G53300) Salk_063943; *ttl2* (AT3G14950) Salk_106516; *ttl3* (AT2G42580) Sail_193_B05; *ttl4* (AT3G58620) Salk_026396; *ttl134*: *ttl1 ttl3 ttl4* triple mutant (Lakhssassi et al., 2012); *bak1-4* (SALK_116202; Chinchilla et al., 2007); *serk1-1* (SALK_044330; Albrecht et al., 2005); *serk1-1 bak1-4* double mutant (obtained by crossing *serk1-1* with *bak1-4*); *bri1-301* (Xu et al., 2008); *ttl134 bri1-301* quadruple mutant (obtained by crossing *ttl134* with *bri1-301*); *bes1-D* (Yin et al., 2002); and *ttl134 bes1-D* quadruple mutant (obtained by crossing *ttl134* with *bes1-D*). Transgenic lines *TTL1p*:*GUS*; *TTL2p*:*GUS*; *TTL3p*:*GUS*, and *TTL4p*:*GUS* (Lakhssassi et al., 2012) were also described previously. Generation of transgenic lines *TTL3-GFP 1.2 (TTL3p*:*TTL3g-GFP* line 1.2 in *ttl3* background) and *TTL3-GFP 2.4 (TTL3p*:*TTL3g-GFP* line 2.4 in *ttl134* background) is described in the section "Generation of Transgenic Plants."

Plant Manipulation and Growth Conditions

Arabidopsis standard handling procedures and conditions were used to promote seed germination and growth. Seeds were surface sterilized and cold treated for 3 d at 4°C. Next, seeds were sowed onto half-strength Murashige and Skoog (MS) agar solidified medium (0.6% [w/v] agar for horizontal growth and 1% [w/v] for vertical growth) containing 1.5% [w/v] Suc, unless otherwise stated. Plates were placed either vertically or horizontally in a culture chamber at 22 ± 1°C, under cool-white light (at 120 μmol photon m^{-2} s^{-1}) with a long-day photoperiod (at 16-h light/8-h dark cycle) unless otherwise stated. When required, seedlings were transferred to soil after 7 d of in vitro growth and watered every 2 d. In soil, plants were grown in a mixture of organic substrate and vermiculite (4:1 [v/v]) under controlled conditions at 23 ± 1°C, 16-h light/8-h dark cycle (at ~120 μmol photon m^{-2} s^{-1}). Freshly harvested seeds were used for all phenotypic analyses.

Plasmid Constructs

A genomic fragment spanning the 1.7-kb *TTL3* promoter (*TTL3p*) region upstream of the start codon and the TTL3 genomic region (*TTL3g*) without stop codon was PCR amplified using the primers detailed in Supplemental Table 1 and cloned into the pCR8 ENTRY vector (Invitrogen).

The coding DNA sequence (CDS) without the stop codon of *TTL3* and *BSK1*, as well as the CDS with the stop codon of the wild-type BRI1 cytoplasmic domain (residues 814 to 1196), BRI1 cytoplasmic domain JMCT9D (BRI1cyt^{JMCT9D} residues 250 to 662), and TTL3 truncated version TTL3ΔN1 (residues 204 to 691), TTL3ΔN2 (residues 371 to 691), TTL3ΔN3 (residues 567 to 691), TTL3ΔC1 (residues 1 to 306), and TTL3ΔC2 (residues 1 to 595) was PCR amplified using the primers detailed in Supplemental Table 1 and cloned into the *pENTR/D-TOPO* vector using the pENTR Directional TOPO cloning kit (Invitrogen). The pUNI51 (Salk Institute) cDNA clone was used as template to PCR amplify the *TTL3* CDS without the stop codon. Total RNA from Arabidopsis Col-0 was used to generate cDNA that was then used as a template to PCR amplify BSK1 CDS without the stop codon. The expression clone pMAC-flag-BRI1-CD-JMCT9D (Wang et al., 2008) was used as template for PCR amplification of BRI1cyt^{JMCT9D}, and it was a gift from Xiaofeng Wang (College of Horticulture Northwest, AandF University, Yangling Shaanxi).

pENTR vectors including CDS without the stop codon of *BRI1*, *BAK1*, *BIN2*, *BSU1*, and *BZR1* were obtained by Gateway BP-reaction (Invitrogen) using an expression clone for each gene of interest (containing *att*B sites) and the pDONR/Zeo vector. Expression clones, used as templates for cloning *BRI1*, *BAK1*, and *BZR1* in the pENTR/D-Topo by Gateway BP-reaction, were published previously (Schwessinger et al., 2011; Lozano-Durán et al., 2014). The expression clones used to clone *BSU1* (Mora-García et al., 2004) and *BIN2* (Bernardo-García et al., 2014) in pENTR/D-Topo by the Gateway BP-reaction were a gift from Santiago Mora Garcia (Fundación Instituto Leloir and Instituto de Investigaciones Bioquímicas de Buenos Aires) and Salomé Prat (Centro Nacional de Biotecnología-Consejo Superior de Investigaciones Cientificas), respectively.

All the resulting pENTR clones were verified by diagnostic PCR, restriction analysis, and sequencing. These pENTR clones in combination with the appropriate destination vectors (pDEST) were used to create the final Gateway-expression constructs by LR-reaction (Invitrogen). The pETG-30A and pETG-30A vectors were provided by the European Molecular Biology Laboratory (EMBL) and were used as pDEST to generate GST and MBP N-terminal fusion proteins for GST-pull-down assays. The pGWB4, pGWB5, pGWB6, and pGWB14, from the pGWB vector series, were provided by Tsuyoshi Nakagawa (Department of Molecular and Functional Genomics, Shimane University; Nakagawa et al., 2007) and were used as pDEST for the transient expression in *Nicotiana Benthamiana* in the Co-IP and coexpression assays (pGWB5, pGWB6, and pGWB14) or for generating stable transgenic Arabidopsis lines (pGWB4). pDEST-GW-VYNE and pDEST-GW-VYCE (Gehl et al., 2009) were used for BiFC assays. The Gateway destination vector pUC19(35S:GW-GFP) and pBSSK(35S:GW-HA) were used to transfect protoplasts for transient expression and Co-IP assays. The pUC19(35S:GW-GFP) vector was provided by José Alonso (Department of Plant and Microbial Biology, North Carolina State University) and contains the pGWB5 cassette between *Hind*III-*Sac*I restriction sites in the pUC19 vector backbone. The pBSSK(35S:GW-HA) vector was generated in this work by cloning the pGWB14 cassette between *Hind*III-*Sac*I in the pBSSK vector backbone. The pGADT7(GW) and pGBKT7(GW) destination vectors were provided by Salomé Prat (Nacional de Biotecnología-Consejo Superior de Investigaciones Cientificas) and used for yeast two-hybrid assay. All the expression clones were verified by diagnostic PCR and restriction analysis.

Generation of Transgenic Plants

Expression constructs were transformed into *Agrobacterium tumefaciens* strain GVG3101::pMP90 through electroporation and confirmed by diagnostic PCR. The pGWB4 harboring the *TTL3p*:*TTL3g-GFP* construct was transformed into Arabidopsis plants by floral dip (Clough and Bent, 1998) to generate stable transgenic plants. *TTL3p*:*TTL3g-GFP* was transformed into both the *ttl3* single mutant and the *ttl134* triple mutant. T3 or T4 homozygous transgenic plants were used in this study.

Venation Pattern Phenotype

Cotyledons (embryonic leaves) from 2-week-old seedlings were cleared and observed under a Nikon AZ100 Multizoom light microscope to analyze vascular patterning, and the percentage of cotyledons displaying each venation pattern categories is depicted in Supplemental Figure 1. Approximately 200 cotyledons per genotype were analyzed. Representative images of each observed venation pattern categories were acquired.

For clearing cotyledons, the 2-week-old seedlings were immersed sequentially in 50% ethanol for 1 h, 99% ethanol overnight, and 50% ethanol for 1 h, and finally transferred to double distilled water. Seedlings were mounted on slides in 50% glycerol and visualized under a light microscope or using the Nikon AZ100 Multizoom microscope system.

Morphological Characterization of Seedlings

Seedlings were grown vertically in long-day photoperiod for 3 d (root analysis) or 7 d (hypocotyl analysis) in half-strength MS agar solidified medium supplemented with 1.5% (w/v) Suc. The root and hypocotyl length of seedlings grown vertically was measured, and the data were analyzed as described in under "Quantification and Statistical Analysis."

eBL Sensitivity Determined by Root Growth Inhibition

Two different BR-inhibition root growth assays were performed to measure BR sensitivity. In the first assay, seedlings were grown vertically in a long-day photoperiod for 4 or 5 d in half-strength MS agar solidified medium supplemented with 1.5% (w/v) Suc and then transferred to half-strength MS agar solidified medium supplemented with 1.5% (w/v) Suc containing either mock (eBL solvent as control) or 100 nM eBL (PhytoTechnology Laboratories) and photographed 6 or 8 d later. In the second assay, seedling were grown vertically in a long-day photoperiod for 7 d in half-strength MS agar solidified medium supplemented with 1.5% (w/v) Suc, containing either mock (eBL solvent as control) or 500 nM eBL (PhytoTechnology Laboratories) and photographed. Root length of seedlings grown for 7 d in the presence of 500 nM eBL was divided by the mean of root length of seedlings grown for 7 d in the absence of BL to calculate the root length fold change.

The eBL (PhytoTechnology Laboratories) was added from a 5 mM stock solution freshly prepared in 80% (v/v) ethanol.

To determine the eBL sensitivity of Col-0 and mutants, the root length of seedlings grown vertically was measured, and the data were analyzed as described under "Quantification and Statistical Analysis."

eBL Sensitivity Determined by Phosphorylation Status of BES1

Seedlings were grown vertically in a long-day photoperiod for 7 d in half-strength MS agar solidified medium supplemented with 1.5% (w/v) Suc and then transferred to half-strength MS liquid medium supplemented with 1.5% (w/v) Suc containing 2.5 μM BRZ (TCI Europe) and grown for three more days. To determine the eBL sensitivity of Col-0 and *ttl134*, the seedlings were treated with either mock (eBL solvent as control) or 10 nM eBL (PhytoTechnology Laboratories) and frozen in liquid nitrogen after 0, 30, and 60 min of treatment. Total protein was extracted as described under "Extraction of Total Protein from Arabidopsis" and analyzed by immunoblotting using an anti-BES1 antibody (dilution 1:500; Yu et al., 2011) as described under "Immunoblot."

Phenotypic Analysis of Hypocotyl Elongation in Dark

Freshly harvested seeds were surface sterilized and cold treated for 3 d at 4°C. Next, seeds were sowed individually onto half-strength MS 1% (p/v) agar solidified medium containing 1.5% Suc for vertical growth. Seedlings were grown for 4 d in long-day photoperiod and then placed in dark conditions (vertical growth in a culture chamber at 22 ± 1°C). Seedlings were photographed, and hypocotyl length was measured 3 d after placing plates in dark conditions.

Total RNA Extraction and Quantitative PCR Analysis

Ten-day-old seedlings (10 seedlings per biological replicate) grown for 5 d on half-strength MS agar solidified medium were transferred to half-strength MS liquid medium supplemented with 1% (w/v) Suc (grown for five extra days) and were used for total RNA extraction. Plant tissue was ground to a fine powder in liquid nitrogen. Approximately 100 mg of ground tissue per sample was homogenized in 1 mL of the commercial reagent TRIsure (Bioline), and total RNA was extracted following the manufacturer's instructions. The RNA concentration and purity were determined spectrophotometrically (Nanodrop ND-1000 spectrophotometer). RNA samples (10 μg per sample) were DNase treated with Turbo DNA-free DNase (Ambion), and 1 μg of RNA per sample was run on a 1% agarose gel to confirm RNA integrity. First-strand cDNA was synthesized from 1 μg of RNA using the iScript cDNA synthesis kit (Bio-Rad), according to the manufacturer's instructions. cDNAs were amplified in triplicate by quantitative PCR (qPCR) using SsoFast EvaGreen supermix (Bio-Rad) and the MyiQ Thermal cycler (Bio-Rad). The relative expression values were determined using *ACTINE2* as a reference gene and plotted relative to Col-0 expression level. Primers used for qPCR are listed in Supplemental Table 2.

Transient Expression in *N. benthamiana*

For transient expression in *N. benthamiana*, *A. tumefaciens* (GV3101::pMP90) carrying the different constructs was used together with the p19 strain for infiltration into 4- to 5-week-old *N. benthamiana* leaves at the abaxial side of the leaf lamina. After infiltration, all plants were kept in the greenhouse and analyzed 2 d later. Agrobacteria cultures were grown overnight in Luria-Bertani medium containing rifampicin (50 μg/mL), gentamycin (25 μg/mL), and the construct-specific antibiotic. Cells were then harvested by centrifugation (for 15 min at 3000*g* in 50-mL falcon tubes) at room temperature, pellets were resuspended in agroinfiltration solution (10 mM MES, pH 5.6, 10 mM $MgCl_2$, and 1 mM acetosyringone), and incubated for 2 h in dark conditions at room temperature. For double infiltration experiments, *Agrobacterium* strains were infiltrated at OD_{600} of 0.4 for the constructs and 0.2 for the p19 strain. For triple infiltration experiments, *Agrobacterium* strains were infiltrated at OD_{600} of 0.26 for the constructs and at OD_{600} of 0.2 for the p19 strain. An *Agrobacterium* strain harboring an empty vector (or β-glucuronidase [GUS]-HA expressing vector) was used to obtain a total OD_{600} of approximately 1 in all the infiltration experiments.

For eBL treatment analysis, leaves were pre-treated with 5 μM BL for 3 h prior to sample collection. *N. benthamiana* leaves were infiltrated with water or 5 μM eBL (PhytoTechnology Laboratories) infiltration solution (10 μL eBL 5mM stock solution in 10 mL of water), made from a 5 mM stock solution freshly prepared in 80% (v/v) ethanol.

Transient Expression in Arabidopsis *NahG* Plants

A. tumefaciens–mediated expression in Arabidopsis NahG plants (Rosas-Díaz et al., 2016) was performed as described for transient expression in *N. benthamiana*, with some modifications. *Agrobacterium* strains were resuspended with an equal OD_{600} in infiltration solution to obtain a total OD_{600} of 0.05 for injection into the abaxial leaf sides of 4- to 5-week-old Arabidopsis plants. At least six plants per co-infiltration mixture and four leaves per plant were used per experiment.

Recombinant Protein Purification and In Vitro Pull-Down Assay

The coding sequences of wild-type BRI1 cytoplasmatic domain (residues 814 to 1196), BRI1 cytoplasmatic domain JMCT9D (residues 250 to 662),

TTL3ΔN1 (residues 204 to 691), and TTL3ΔN3 (residues 567 to 691) were cloned as described under "Plasmid Constructs" to generate MBP-BRI1cyt, MBP-BRI1cyt^{JMCT9D}, GST-TTL3ΔN1, and GST-TTL3ΔN3 constructs. Recombinant proteins were expressed in *Escherichia coli* strain BL21 (DE3) and extracted using buffer A (140 mM NaCl, 2.7 mM KCl, 10 mM Na_2HPO_4, 1.8 mM KH_2PO_4, and 1% Triton X-100, pH 8, supplemented with 1 mM phenylmethylsulfonyl fluoride [PMSF], 0.2 μL/10 mL Benzonase Nuclease [Sigma-Aldrich], and 1 mg/mL Lisozyme). MBP and GST fusion proteins were purified with glutathione Sepharose 4B GST-tagged protein purification resin (GE Healthcare) or MBP binding protein coupled to agarose beads (MBP-Trap_A, Chromotek), respectively, according to the manufacturers' instructions.

To investigate protein–protein interactions, the GST-tagged proteins were first captured by the glutathione agarose–coated beads and then incubated with the MBP-tagged proteins in dilution/wash buffer (50 mM Tris-HCl, pH 7.5, 150 mM NaCl, 10% glycerol, 10 mM EDTA, pH 8, 10 mM DTT, 0.5 mM PMSF, and 1% [v/v] P9599 protease inhibitor cocktail [Sigma-Aldrich]) at 4°C for 1 h in an end-over-end rocker. Protein–protein interaction complexes bound to the glutathione agarose–coated beads were pulled down, washed three times with the dilution/wash buffer and analyzed by immunoblot as described under "Immunoblot."

Immunoblotted GST- and MBP-tagged protein was detected using an anti-GST antibody (catalog no. G7781, Sigma-Aldrich; dilution 1:10,000) and a specific anti-BRI1 antibody (dilution 1:2000; Bojar et al., 2014) as described in the section "Immunoblot."

Protein Extraction and Co-IP in *N. benthamiana*

Protein extraction and Co-IP in *N. benthamiana* were performed as described previously (Kadota et al., 2016), with some modifications. Briefly, 4-week-old *N. benthamiana* plants were used for transient expression assays as described under "Transient Expression in *N. benthamiana*." Leaves were ground to fine powder in liquid nitrogen. Approximated 0.5 g of ground leaves per sample was used, and total proteins were then extracted with extraction buffer (50 mM Tris-HCl, pH 7.5, 150 mM NaCl, 10% glycerol, 10 mM EDTA, pH 8, 1 mM NaF, 1 mM $Na_2MoO_4 \cdot 2H_2O$, 10 mM DTT, 0.5 mM PMSF, 1% [v/v] P9599 protease inhibitor cocktail [Sigma-Aldrich]); Nonidet P-40, CAS: 9036-19-5 [USB Amersham Life Science] 0.5% (v/v) for Co-IP involving transmembrane proteins BRI1 and BAK1, and 0.2% [v/v] for the rest of Co-IP) added at 2 mL/g powder using an end-over-end rocker for 30 min at 4°C. Samples were centrifuged 20 min at 4°C and 9000 rpm (9056*g*). Supernatants (~4 mg/mL protein) were filtered by gravity through Poly-Prep chromatography columns (731-1550, Bio-Rad), and 100 μL was reserved for immunoblot analysis as input. The remaining supernatants were incubated for 2 h at 4°C with 15 μL of GFP-Trap coupled to agarose beads (Chromotek) in an end-over-end rocker. During incubation of protein samples with GFP-Trap beads, the final concentration of detergent (Nonidet P-40) was adjusted to 0.2% (v/v) in all cases to avoid unspecific binding to the matrix as recommended by the manufacturer. Following incubation, the beads were collected and washed four times with the wash buffer (similar to extraction buffer but without detergent). Finally, beads were resuspended in 75 μL of 2× concentrated Laemmli sample buffer and heated at 60°C for 30 min (for Co-IP involving transmembrane proteins BRI1 and BAK1) or at 70°C for 20 min (for the remaining Co-IPs) to dissociate immunocomplexes from the beads. Total (input), immunoprecipitated (IP), and CoIP proteins were separated in a 10% SDS-PAGE gel and analyzed as described in the section "Immunolot."

BiFC Assays

Leaves were co-agroinfiltrated as described in the section "*Agrobacterium*-Mediated Transient Expression in *N. benthamiana*" with the *Agrobacterium* strain harboring a construct to express a given protein (Protein A) fused to the N-terminal half of YFP (Protein A-nYFP) and the BiFC partner protein (Protein B) fused to the C-terminal half of YFP (Protein B-cYFP), and vice versa (Protein A-cYFP and Protein B-nYFP) to test both BiFC directions. Leaves were observed using a confocal microscope 2 d after infiltration, as described in the section "Confocal Imaging of Arabidopsis and *N. benthamiana*."

Confocal Imaging of Arabidopsis and *N. benthamiana*

Arabidopsis seedlings were germinated in half-strength MS agar solidified medium (1% [w/v] agar for vertical growth) supplemented with 1.5% Suc. For eBL treatment analysis, 4-d-old seedlings were incubated in 2 mL of half-strength MS medium supplemented with 1.5% (w/v) Suc containing either mock (eBL solvent as control) or 1 μM eBL (PhytoTechnology Laboratories). For BRZ/eBL treatment analysis, 3-d-old seedlings were incubated in 2 mL of half-strength MS medium supplemented with 1% (w/v) Suc, containing either mock (BRZ solvent as control) or 5 μM BRZ (TCI Europe) for 12 h (overnight). The next morning, samples were further treated with mock or 1 μM eBL (PhytoTechnology Laboratories) for another 1 h before being analyzed by confocal microcopy. The eBL (PhytoTechnology Laboratories) and BRZ (TCI Europe) were added from a 5 mM stock solution freshly prepared in 80% (v/v) ethanol. For visualization of plasma membrane, seedlings were incubated in 1 mL of double distilled water containing 1 μg/mL FM4-64 (Invitrogen Molecular Probes) prepared from a 1 mg/mL stock solution for 3 to 4 min, rinsed in double distilled water to remove the excess stain, and visualized under confocal microscopy.

For confocal imaging of *N. benthamiana* leaves in coexpression and BiFC experiments, GFP or YFP fluorescence of the lower epidermis of the leaf was visualized with the confocal 2 d after infiltration.

Confocal imaging of Arabidopsis *NahG* plants was performed as described for *N. benthamiana*, but in this case, images are a maximum Z-projection of seven 1-μm spaced confocal planes from the cell equatorial plane to the cell surface.

All confocal images were obtained using a Leica TCS SP5 II confocal microscope equipped with a 488-nm argon laser for GFP and YFP and a 561-nm He-Ne laser for FM4-64. Leica LAS AF Lite platform and the Java-based image-processing program FIJI (Schindelin et al., 2012; Schneider et al., 2012) were used in the processing of all microscopy images.

Stereo Microscopy of Arabidopsis Seedlings

Representative images of Arabidopsis seedlings were acquired using the Nikon Eclipse Ti basic fluorescence microscope system with a filter for GFP or ZEISS SteREO Discovery V12 with digital cam Axiocam 503 color (excitation wavelengths 488 and emission wavelengths 498 to 550). Wild-type Col-0 Arabidopsis seedlings were used as a negative control for chlorophyll fluorescence.

GUS Staining Assay

Four-day-old seedlings were transferred to a medium containing 0.2 μM eBL (PhytoTechnology Laboratories) for 24 h and then stained for GUS activity. Plant tissues were immersed in histochemical GUS staining buffer (100 mM $NaPO_4$, pH 7, 0.5 mM $K_3[Fe(CN)_6]$, 0.5 mM $K_4[Fe(CN)_6]$, 20% methanol, 0.3% Triton X-100, and 2 mM 5-bromo-4-chloro-3-indoxyl-β-D-glucuronide cyclohexylammonium [Gold Biotechnology]) in multi-well plates, vacuum infiltrated (60 cm Hg) for 10 min three times, and then wrapped in aluminum foil and incubated at 37°C for 12 h. Samples were then washed several times with 95% ethanol until complete tissue clarification, stored in 50% glycerol, and photographed using the Nikon AZ100 Multizoom microscope system.

Protoplast Transient Expression Assays

Protoplast extraction and transfection were performed as described previously (Yoo et al., 2007). Briefly, leaves from 5-week-old Arabidopsis Col-0 plants grown under a 10-h daylight photoperiod were cut into very small strips and digested for 3 h in the darkness at room temperature. Protoplasts were then washed and resuspended to a concentration of 5×10^5 protoplasts/mL before polyethylene glycol–mediated transfection for 10 min. Twenty microliters of plasmid expressing GFP or 100 μL of plasmid expressing TTL3-GFP/BZR1-HA was used to transfect 2 mL of protoplasts for each transfection. All the plasmids were used at a concentration of 1 μg/μL. The transfected protoplasts were incubated for 6 h at room temperature and collected for protein extraction and immunoprecipitation, as described for *N. benthamiana* samples.

Yeast Two-Hybrid Assay

The Gal4-based yeast two-hybrid system (Clontech Laboratories) was used for testing the interaction between TTL3 and different components of the BR signaling pathway. The bait and prey constructs are explained under "Plasmid Constructs." The bait and prey plasmids were transformed into *Saccharomyces cerevisiae* strain AH109 as described previously (Gietz and Schiestl, 1995), and transformants were grown on plasmid-selective media (synthetic defined (SD)/−Trp−Leu). Plates were incubated at 28°C for 4 d and independent colonies for each bait–prey combination were resuspended in 200 μL of sterile water. Tenfold serial dilutions were made and 5 μL of each dilution were spotted onto three alternative interaction-selective medium (SD/−Trp−Leu−His+3-AT (for 3-amino-1,2,4-triazole, 2mM), SD/−Trp−Leu−Ade, and SD/−Trp−Leu−Ade+3-AT). Plates were incubated at 28°C and photographed 3 or 7 d later.

Yeast Two-Hybrid Protein Extraction

For immunoblot analysis, one or two independent yeast cotransformants (a and b) for each bait–prey plasmid combination were grown in 50 mL of SD/−Leu−Trp to an OD_{600} of 0.7 to 1. Cultures were centrifuged at 4000 rpm for 3 min. The resulting pellet was washed once with cold water and resuspended in 200 μL of RIPA buffer (2 mM sodium phosphate buffer, pH 7, 0.2% Triton X-100, 0.02% [w/v] SDS, 0.2 mM EDTA, pH 8, and 10 mM NaCl) containing protease inhibitor (1 tablet/10 mL, cOmplete, Mini, EDTA-free Protease Inhibitor Cocktail, Roche). Glass beads (500 μL, 425 to 600 μm, Sigma-Aldrich) were added, and the sample was vortexed in FastPrepTM FP120 (BIO 101) at a power setting of 5.5 for two 15-s intervals separated by 1-min interval on ice. Next, 400 μL of RIPA buffer with protease inhibitors was added, and the sample was vigorously vortexed. The supernatant was recovered, and the protein concentration was determined using Bradford assays. Total protein (50 μg) was resolved on 10% polyacrylamide/SDS gels and analyzed by immunoblotting using an anti-Myc Tag (1:2000, Abgent), which is transcriptionally fused to Gal4BD, as described in the section "Immunoblot."

Extraction of Total Protein from Arabidopsis

Arabidopsis tissue was ground to a fine powder in liquid nitrogen. Approximately 100 mg of ground tissue per sample was used for total protein extraction. Denatured protein extracts were obtained by homogenizing and incubating plant material in 200 μL of 2× Laemmli buffer (125 mM Tris-HCl, pH 6.8, 4% [w/v] SDS, 20% [v/v] glycerol, 2% [v/v] β-mercaptoethanol, and 0.01% [w/v] bromophenol blue) for 5 min at 95°C, centrifuged (for 5 min at 20,000*g*) at room temperature, and the total proteins from supernatant were separated in a 10% SDS-PAGE gel and analyzed as described in the section "Immunoblot."

Immunoblot

Proteins separated by SDS-PAGE polyacrylamide gel electrophoresis were electroblotted using Trans-blot Turbo Transfer System (Bio-Rad) onto polyvinylidene difluoride (PVDF) membranes (Immobilon-P, Millipore) following instructions by the manufacturer (preprogramed protocols optimized for the molecular weight of the proteins of interest). PVDF membranes, containing electroblotted proteins, were then incubated with the appropriate primary antibody followed by the appropriate secondary peroxidase-conjugated antibody. In addition to the primary antibodies described in the previous methods section, the following primary antibodies were used for detection of epitope-tagged proteins: mouse monoclonal anti-GFP clone B-2 (1:600, catalog no. sc-9996, lot no. C0619, Santa Cruz Biotechnology), mouse monoclonal anti-HA clone HA-7 (1:3000, catalog no. H3663, Sigma-Aldrich), and mouse monoclonal anti-myc clone 9E10 (1:2000, catalog no. AM1007a, Abgent). The secondary antibodies used in this study were as follows: anti-mouse IgG whole molecule−Peroxidase (1:80,000; catalog no. A9044, lot no. 031M4752, Sigma-Aldrich) and anti-rabbit IgG whole molecule−Peroxidase (1:80,000; catalog no. A0545, lot no. 026M4782V, Sigma-Aldrich).

Proteins and epitope-tagged proteins on immunoblots were detected using the Clarity ECL Western Blotting Substrate or SuperSignal West Femto Maximum Sensitivity Substrate according to the manufacturer's instructions, and images of different time exposures were acquired using the Chemidoc XRS+System (Bio-Rad). SDS-PAGE polyacrylamide gels and immunoblotted PVDF membranes were stained with Coomassie Brilliant Blue R 250 to confirm equal loading of the different samples in a given experiment.

QUANTIFICATION AND STATISTICAL ANALYSIS

Arabidopsis eFP Browser Data Analysis

Gene expression level data from hormone responses were retrieved from the Arabidopsis eFP Browser (Hormone Series) website (http://bar.utoronto.ca/efp/cgi-bin/efpWeb.cgi; Winter et al., 2007). Data used for the analysis were obtained from 7-d-old wild-type seedlings. Differential expression was calculated by dividing the expression value of each gene in a given hormone treatment by the corresponding mock control (fold change of hormone treatment relative to the mock). The hormone gene expression response was calculated and the heatmap was created using Excel (Microsoft). In the heatmap, red represents induction and blue represents repression as response to the indicated hormone.

Quantification of Fluorescent Protein Signal

For quantification of fluorescent protein signal in plasma membrane versus cytoplasm, all images were analyzed using FIJI software (Schindelin et al., 2012; Schneider et al., 2012). To measure the ratio between nuclear and cytoplasmic signals, a small area of fixed size (8 pixels) was drawn, and measurements of integrated densities were taken from representative areas within the plasma membrane and cytoplasm of each cell. To delineate the plasma membrane area, FM4-64 was used to stain the cells. Average ratios between plasma membrane and cytoplasmic signal intensities were calculated based on measurements from three cells per plant; $n = 10$ plants analyzed (three cells per plant). This experiment was repeated twice with similar results.

Additionally, for quantification of fluorescent protein signal, line scan measurements spanning membrane and cytoplasm were performed from images using FIJI software (Schindelin et al., 2012; Schneider et al., 2012), and representative plot profiles of sample measurements are presented in Figure 4I.

The quantification the BiFC fluorescence intensity of BSK1 and BZR1 in the presence or absence of TTL3-HA (Figure 7B) was performed using FIJI software (Schindelin et al., 2012; Schneider et al., 2012). The area in pixels and raw integrated density of the fluorescence signal were measured in at least five randomly chosen regions of infiltrated leaves per experiment. Fluorescence intensity (arbitrary units) was calculated by dividing the raw integrated density by the area in pixels of the fluorescence signal.

Statistics

Band intensity quantification of protein signal detected by immunoblot, integrated densities from representative areas within the plasma membrane and cytoplasm of each cell analyzed by confocal imaging, and Arabidopsis root and hypocotyl lengths were measured from images using FIJI software (Schindelin et al., 2012; Schneider et al., 2012). The data for qRT-PCR were gathered with MyiQ optical system software (Bio-Rad). For statistical analysis, unpaired *t* test or one-way analysis of variance (ANOVA) followed by Tukey's multiple comparison test ($P < 0.05$) was performed using Prism 6.00 for Mac (GraphPad Software, www.graphpad.com). ANOVA and/or *t* test results for the data presented in each figure are detailed in the Supplemental Data Set. Asterisks indicate statistical differences between mutant versus Col-0, unless otherwise specified, as determined by the unpaired *t* test (*$P \leq 0.05$, **$P \leq 0.01$, ***$P \leq 0.001$, ****$P \leq 0.0001$). Different lowercase letters in the graphs indicate significant differences. Data represent mean values and error bars are SEM. In figure legends, *n* means number of plants for phenotypic analysis, numbers of biological replicates (three technical replicates per biological replicate) for qPCR analysis, or number of cells (three independent measurements performed per cell) analyzed for quantification of fluorescent protein signal in plasma membrane versus cytoplasm. The experiments were repeated at least three times with similar results.

In Silico Three-Dimensional Structural Model of TTL3

The in silico protein structure prediction for TTL3 protein was built by submitting primary sequences to the I-TASSER server (Zhang, 2008) and processed by PyMOL (Schrödinger). IDRs were predicted using GlobPlot 2 (http://globplot.embl.de/). TPR and thioredoxin-like (TPRX) domains were predicted using the SMART/Pfam server and were described previously (Lakhssassi et al., 2012).

Accession Numbers

Sequence data from this article can be found in the EMBL/GenBank data libraries under the following accession numbers: AT1G53300 for *TTL1*, AT3G14950 for *TTL2*, AT2G42580 for *TTL3*, AT3G58620 for *TTL4*, AT4G33430 for *BAK1*, AT1G71830 for *SERK1*, AT4G39400 for *BRI1*, AT2G01950 for *BRL2*, AT4G35230 for *BSK1*, AT1G03445 for *BSU1*, AT4G18710 for *BIN2*, AT1G75080 for *BZR1*, AT1G19350 for *BES1*.

Supplemental Data

Supplemental Figure 1. *TTL* genes are required for cotyledon vein pattern formation. Supports Figure 1.

Supplemental Figure 2. TTL3 presents an intrinsically disorder region (IDR) at the N terminus. Supports Figure 1.

Supplemental Figure 3. Protein sequence alignment of BRI1 and BRL2 cytoplasmic domain. Supports Figure 1.

Supplemental Figure 4. Purified GST- and MBP-fused proteins used for the GST Pull-down assays. Supports Figure 1.

Supplemental Figure 5. TTL3 specifically associates with BRI1, but not with BAK1 or free GFP. Supports Figure 1.

Supplemental Figure 6. TTL3 associates with BSK1, BSU1, BIN2, and BZR1 in BiFC experiments. Supports Figures 1, 5, and 6.

Supplemental Figure 7. The expression of *TTL1*, *TTL3*, and *TTL4* are specifically induced by BRs. Supports Figures 2 and 3.

Supplemental Figure 8. *TTL1*, *TTL3*, and *TTL4* genes play a positive role in BR signaling. Supports Figure 2.

Supplemental Figure 9. Mutations in *TTL1*, *TTL3*, and *TTL4* aggravate the weak *bri1-301* phenotype and alleviate part of the *bes1-D* phenotypes. Supports Figure 3.

Supplemental Figure 10. TTL3 presents a cytoplasmic/plasma membrane sub-cellular localization. Supports Figure 4.

Supplemental Figure 11. *TTL3-GFP* 1.2 complements the root length phenotype of *ttl3* in response to eBL treatment. Supports Figure 4.

Supplemental Figure 12. Immunoblot analyses revel that eBL treatment induces TTL3-GFP protein stabilization and that there are no degradation-products of TTL3-GFP in the Arabidopsis TTL3-GFP 2.4 line. Supports Figure 4.

Supplemental Figure 13. BRs regulate the cytoplasmic/plasma membrane localization of TTL3. Supports Figure 4.

Supplemental Figure 14. TTL3 N terminus negatively affects the stabilization of TTL3 in yeast heterologous system. Supports Figures 5 and 6.

Supplemental Figure 15. TTL3 preferentially associates with the phosphorylated form of BZR1 by Co-IP and regulates its cytoplasmic/nuclear localization. Supports Figure 6.

Supplemental Figure 16. BSK1 co-immunoprecipitates with BZR1. Supports Figure 7.

Supplemental Table 1. List and description of primers used for cloning into pENTR.

Supplemental Table 2. List of primers used for quantitative RT-PCR.

Supplemental Data Set. Statistical report of *t* tests and ANOVAs results for the data presented in each figure.

ACKNOWLEDGMENTS

We thank Yanhai Yin and Michael Hothorn for generously providing the anti-BES1 and the anti-BRI1 antibodies, respectively. We thank Salomé Prat (*BIN2* expression clone), Santiago Mora Garcia (BSU1 expression clone), José Alonso (GFP-tagged GW vector for expression in protoplasts), and Xiaofeng Wang (pMAC-flag-BRI1-CD-JMCT9D, BRI1 phosphomimetic mutant) for providing expression clones and vectors.

This work was supported by the Ministerio de Economía y Competitividad (cofinanced by the European Regional Development Fund) (grant BIO2017-82609-R to M.A.B.) and by a Formación del Personal Investigador Fellowship from the Ministerio de Economía y Competitividad (FPI-BES 2015-071256 to A.G.-M.), by the Shanghai Center for Plant Stress Biology (Chinese Academy of Sciences), Chinese 1000 Talents Program (to A.P.M.), and by the Gatsby Charitable Foundation and the European Research Council (grant 309858 "PHOSPHinnATE" to C.Z.). Support was also provided by the Ramón y Cajal Program (RYC-2013-12699 MINECO-Universidad de Málaga, Spain to D.P.); by a fellowship from Agencia Española de Cooperación Internacional para el Desarrollo (Ministerio de Asuntos Exteriores y Cooperacion); and by the Ministerio de Educacion y Ciencia (Universidad de Málaga, Spain) to N.L.

AUTHOR CONTRIBUTIONS

All authors (V.A.-S., A.G.-M., A.G.C., N.L., J.P.-S., Y.L., A.E.d.V., D.P., J.P.-R., A.P.M., V.V., O.B., and C.Z.) designed the experiments. V.A.-S., A.G.-M., A.G.C., N.L., J.P.-S., Y.L., A.E.d.V., D.P., J.P.-R., and A.P.M. performed the experiments and analyzed the data. V.A.-S., A.P.M., and M.A.B. wrote the article. All authors commented on the article.

Received March 8, 2019; revised May 7, 2019; accepted May 31, 2019; published June 12, 2019.

REFERENCES

Albrecht, C., Russinova, E., Hecht, V., Baaijens, E., and de Vries, S. (2005). The *Arabidopsis thaliana* SOMATIC EMBRYOGENESIS RECEPTOR-LIKE KINASES1 and 2 control male sporogenesis. Plant Cell **17:** 3337–3349.

Belkhadir, Y., and Jaillais, Y. (2015). The molecular circuitry of brassinosteroid signaling. New Phytol. **206:** 522–540.

Bernardo-García, S., de Lucas, M., Martínez, C., Espinosa-Ruiz, A., Davière, J.-M., and Prat, S. (2014). BR-dependent phosphorylation modulates PIF4 transcriptional activity and shapes diurnal hypocotyl growth. Genes Dev. **28:** 1681–1694.

Blatch, G.L., and Lässle, M. (1999). The tetratricopeptide repeat: A structural motif mediating protein-protein interactions. Bioessays **21:** 932–939.

Bojar, D., Martinez, J., Santiago, J., Rybin, V., Bayliss, R., and Hothorn, M. (2014). Crystal structures of the phosphorylated BRI1 kinase domain and implications for brassinosteroid signal initiation. Plant J. **78:** 31–43.

Cai, Z., Liu, J., Wang, H., Yang, C., Chen, Y., Li, Y., Pan, S., Dong, R., Tang, G., Barajas-Lopez, J. de D., Fujii, H., and Wang, X. (2014). GSK3-like kinases positively modulate abscisic acid signaling through phosphorylating subgroup III SnRK2s in Arabidopsis. Proc. Natl. Acad. Sci. USA **111:** 9651–9656.

Caño-Delgado, A., Yin, Y., Yu, C., Vafeados, D., Mora-García, S., Cheng, J.-C., Nam, K.H., Li, J., and Chory, J. (2004). BRL1 and BRL3 are novel brassinosteroid receptors that function in vascular differentiation in Arabidopsis. Development **131:** 5341–5351.

Ceserani, T., Trofka, A., Gandotra, N., and Nelson, T. (2009). VH1/BRL2 receptor-like kinase interacts with vascular-specific adaptor proteins VIT and VIK to influence leaf venation. Plant J. **57:** 1000–1014.

Chaiwanon, J., Wang, W., Zhu, J.-Y., Oh, E., and Wang, Z.-Y. (2016). Information integration and communication in plant growth regulation. Cell **164:** 1257–1268.

Chinchilla, D., Zipfel, C., Robatzek, S., Kemmerling, B., Nürnberger, T., Jones, J.D.G., Felix, G., and Boller, T. (2007). A flagellin-induced complex of the receptor FLS2 and BAK1 initiates plant defence. Nature **448:** 497–500.

Chung, Y., and Choe, S. (2013). The regulation of brassinosteroid biosynthesis in Arabidopsis. Crit. Rev. Plant Sci. **32:** 396–410.

Clough, S.J., and Bent, A.F. (1998). Floral dip: A simplified method for *Agrobacterium*-mediated transformation of *Arabidopsis thaliana*. Plant J. **16:** 735–743.

D'Andrea, L.D., and Regan, L. (2003). TPR proteins: The versatile helix. Trends Biochem. Sci. **28:** 655–662.

Du, J., Yin, H., Zhang, S., Wei, Z., Zhao, B., Zhang, J., Gou, X., Lin, H., and Li, J. (2012). Somatic embryogenesis receptor kinases control root development mainly via brassinosteroid-independent actions in *Arabidopsis thaliana*. J. Integr. Plant Biol. **54:** 388–399.

Fàbregas, N., Li, N., Boeren, S., Nash, T.E., Goshe, M.B., Clouse, S.D., de Vries, S., and Caño-Delgado, A.I. (2013). The brassinosteroid insensitive1-like3 signalosome complex regulates Arabidopsis root development. Plant Cell **25:** 3377–3388.

Gampala, S.S., et al. (2007). An essential role for 14-3-3 proteins in brassinosteroid signal transduction in Arabidopsis. Dev. Cell **13:** 177–189.

Gehl, C., Waadt, R., Kudla, J., Mendel, R.R., and Hänsch, R. (2009). New GATEWAY vectors for high throughput analyses of protein-protein interactions by bimolecular fluorescence complementation. Mol. Plant **2:** 1051–1058.

Geldner, N., Hyman, D.L., Wang, X., Schumacher, K., and Chory, J. (2007). Endosomal signaling of plant steroid receptor kinase BRI1. Genes Dev. **21:** 1598–1602.

Gietz, R.D., and Schiestl, R.H. (1995). Transforming yeast with DNA (invited chapter). Methods Mol. Cell. Biol. **5:** 255–269.

González-García, M.-P., Vilarrasa-Blasi, J., Zhiponova, M., Divol, F., Mora-García, S., Russinova, E., and Caño-Delgado, A.I. (2011). Brassinosteroids control meristem size by promoting cell cycle progression in Arabidopsis roots. Development **138:** 849–859.

Gou, X., Yin, H., He, K., Du, J., Yi, J., Xu, S., Lin, H., Clouse, S.D., and Li, J. (2012). Genetic evidence for an indispensable role of somatic embryogenesis receptor kinases in brassinosteroid signaling. PLoS Genet. **8:** e1002452.

Habchi, J., Tompa, P., Longhi, S., and Uversky, V.N. (2014). Introducing protein intrinsic disorder. Chem. Rev. **114:** 6561–6588.

He, J.X., Gendron, J.M., Yang, Y., Li, J., and Wang, Z.Y. (2002). The GSK3-like kinase BIN2 phosphorylates and destabilizes BZR1, a positive regulator of the brassinosteroid signaling pathway in Arabidopsis. Proc. Natl. Acad. Sci. USA **99:** 10185–10190.

He, K., Gou, X., Yuan, T., Lin, H., Asami, T., Yoshida, S., Russell, S.D., and Li, J. (2007). BAK1 and BKK1 regulate brassinosteroid-dependent growth and brassinosteroid-independent cell-death pathways. Curr. Biol. **17:** 1109–1115.

Houbaert, A., et al. (2018). POLAR-guided signalling complex assembly and localization drive asymmetric cell division. Nature **563:** 574–578.

Jaillais, Y., and Vert, G. (2016). Brassinosteroid signaling and BRI1 dynamics went underground. Curr. Opin. Plant Biol. **33:** 92–100.

Kadota, Y., Macho, A.P., and Zipfel, C. (2016). Immunoprecipitation of plasma membrane receptor-like kinases for identification of phosphorylation sites and associated proteins. In Methods in Molecular Biology (New York: Springer), pp. 133–144.

Kim, T.-W., and Wang, Z.-Y. (2010). Brassinosteroid signal transduction from receptor kinases to transcription factors. Annu. Rev. Plant Biol. **61:** 681–704.

Kim, T.-W., Guan, S., Sun, Y., Deng, Z., Tang, W., Shang, J.-X., Sun, Y., Burlingame, A.L., and Wang, Z.-Y. (2009). Brassinosteroid signal transduction from cell-surface receptor kinases to nuclear transcription factors. Nat. Cell Biol. **11:** 1254–1260.

Kim, T.-W., Michniewicz, M., Bergmann, D.C., and Wang, Z.-Y. (2012). Brassinosteroid regulates stomatal development by GSK3-mediated inhibition of a MAPK pathway. Nature **482:** 419–422.

Kudla, J., and Bock, R. (2016). Lighting the way to protein-protein interactions: Recommendations on best practices for bimolecular fluorescence complementation analyses. Plant Cell **28:** 1002–1008.

Lachowiec, J., Lemus, T., Thomas, J.H., Murphy, P.J.M., Nemhauser, J.L., and Queitsch, C. (2013). The protein chaperone HSP90 can facilitate the divergence of gene duplicates. Genetics **193:** 1269–1277.

Lakhssassi, N., Doblas, V.G., Rosado, A., del Valle, A.E., Posé, D., Jimenez, A.J., Castillo, A.G., Valpuesta, V., Borsani, O., and Botella, M.A. (2012). The Arabidopsis tetratricopeptide thioredoxin-like

gene family is required for osmotic stress tolerance and male sporogenesis. Plant Physiol. **158:** 1252–1266.

Li, J., Wen, J., Lease, K.A., Doke, J.T., Tax, F.E., and Walker, J.C. (2002). BAK1, an Arabidopsis LRR receptor-like protein kinase, interacts with BRI1 and modulates brassinosteroid signaling. Cell **110:** 213–222.

Lin, W., Lu, D., Gao, X., Jiang, S., Ma, X., Wang, Z., Mengiste, T., He, P., and Shan, L. (2013). Inverse modulation of plant immune and brassinosteroid signaling pathways by the receptor-like cytoplasmic kinase BIK1. Proc. Natl. Acad. Sci. USA **110:** 12114–12119.

Lozano-Durán, R., and Zipfel, C. (2015). Trade-off between growth and immunity: Role of brassinosteroids. Trends Plant Sci. **20:** 12–19.

Lozano-Durán, R., Bourdais, G., He, S.Y., and Robatzek, S. (2014). The bacterial effector HopM1 suppresses PAMP-triggered oxidative burst and stomatal immunity. New Phytol. **202:** 259–269.

Ma, X., Xu, G., He, P., and Shan, L. (2016). SERKing coreceptors for receptors. Trends Plant Sci. **21:** 1017–1033.

Maselli, G.A., Slamovits, C.H., Bianchi, J.I., Vilarrasa-Blasi, J., Caño-Delgado, A.I., and Mora-García, S. (2014). Revisiting the evolutionary history and roles of protein phosphatases with Kelch-like domains in plants. Plant Physiol. **164:** 1527–1541.

Mora-García, S., Vert, G., Yin, Y., Caño-Delgado, A., Cheong, H., and Chory, J. (2004). Nuclear protein phosphatases with Kelch-repeat domains modulate the response to brassinosteroids in Arabidopsis. Genes Dev. **18:** 448–460.

Nakagawa, T., Kurose, T., Hino, T., Tanaka, K., Kawamukai, M., Niwa, Y., Toyooka, K., Matsuoka, K., Jinbo, T., and Kimura, T. (2007). Development of series of gateway binary vectors, pGWBs, for realizing efficient construction of fusion genes for plant transformation. J. Biosci. Bioeng. **104:** 34–41.

Nam, K.H., and Li, J. (2002). BRI1/BAK1, a receptor kinase pair mediating brassinosteroid signaling. Cell **110:** 203–212.

Nolan, T.M., Brennan, B., Yang, M., Chen, J., Zhang, M., Li, Z., Wang, X., Bassham, D.C., Walley, J., and Yin, Y. (2017). Selective autophagy of BES1 mediated by DSK2 balances plant growth and survival. Dev. Cell **41:** 33–46.

Peng, P., Yan, Z., Zhu, Y., and Li, J. (2008). Regulation of the Arabidopsis GSK3-like kinase BRASSINOSTEROID-INSENSITIVE 2 through proteasome-mediated protein degradation. Mol. Plant **1:** 338–346.

Prasad, B.D., Goel, S., and Krishna, P. (2010). In silico identification of carboxylate clamp type tetratricopeptide repeat proteins in Arabidopsis and rice as putative co-chaperones of Hsp90/Hsp70. PLoS One **5:** e12761.

Ren, H., Willige, B.C., Jaillais, Y., Geng, S., Park, M.Y., Gray, W.M., and Chory, J. (2019). BRASSINOSTEROID-SIGNALING KINASE 3, a plasma membrane-associated scaffold protein involved in early brassinosteroid signaling. PLoS Genet. **15:** e1007904.

Rosado, A., Schapire, A.L., Bressan, R.A., Harfouche, A.L., Hasegawa, P.M., Valpuesta, V., and Botella, M.A. (2006). The Arabidopsis tetratricopeptide repeat-containing protein TTL1 is required for osmotic stress responses and abscisic acid sensitivity. Plant Physiol. **142:** 1113–1126.

Rosas-Díaz, T., Cana-Quijada, P., Amorim-Silva, V., Botella, M.A., Lozano-Durán, R., and Bejarano, E.R. (2016). Arabidopsis NahG plants as a suitable and efficient system for transient expression using *Agrobacterium tumefaciens*. Mol. Plant. Mol. Plant **10:** 353–356.

Ryu, H., Kim, K., Cho, H., Park, J., Choe, S., and Hwang, I. (2007). Nucleocytoplasmic shuttling of BZR1 mediated by phosphorylation is essential in Arabidopsis brassinosteroid signaling. Plant Cell **19:** 2749–2762.

Samakovli, D., Margaritopoulou, T., Prassinos, C., Milioni, D., and Hatzopoulos, P. (2014). Brassinosteroid nuclear signaling recruits HSP90 activity. New Phytol. **203:** 743–757.

Schindelin, J., et al. (2012). Fiji: an open-source platform for biological-image analysis. Nat. Methods **9:** 676–682.

Schneider, C.A., Rasband, W.S., and Eliceiri, K.W. (2012). NIH Image to ImageJ: 25 years of image analysis. Nat. Methods **9:** 671–675.

Schwessinger, B., Roux, M., Kadota, Y., Ntoukakis, V., Sklenar, J., Jones, A., and Zipfel, C. (2011). Phosphorylation-dependent differential regulation of plant growth, cell death, and innate immunity by the regulatory receptor-like kinase BAK1. PLoS Genet. **7:** e1002046.

Shi, H., Shen, Q., Qi, Y., Yan, H., Nie, H., Chen, Y., Zhao, T., Katagiri, F., and Tang, D. (2013). BR-SIGNALING KINASE1 physically associates with FLAGELLIN SENSING2 and regulates plant innate immunity in Arabidopsis. Plant Cell **25:** 1143–1157.

Shigeta, T., Zaizen, Y., Asami, T., Yoshida, S., Nakamura, Y., Okamoto, S., Matsuo, T., and Sugimoto, Y. (2014). Molecular evidence of the involvement of heat shock protein 90 in brassinosteroid signaling in Arabidopsis T87 cultured cells. Plant Cell Rep. **33:** 499–510.

Shigeta, T., Zaizen, Y., Sugimoto, Y., Nakamura, Y., Matsuo, T., and Okamoto, S. (2015). Heat shock protein 90 acts in brassinosteroid signaling through interaction with BES1/BZR1 transcription factor. J. Plant Physiol. **178:** 69–73.

Shimada, S., Komatsu, T., Yamagami, A., Nakazawa, M., Matsui, M., Kawaide, H., Natsume, M., Osada, H., Asami, T., and Nakano, T. (2015). Formation and dissociation of the BSS1 protein complex regulates plant development via brassinosteroid signaling. Plant Cell **27:** 375–390.

Soutourina, J. (2018). Transcription regulation by the Mediator complex. Nat. Rev. Mol. Cell Biol. **19:** 262–274.

Sreeramulu, S., Mostizky, Y., Sunitha, S., Shani, E., Nahum, H., Salomon, D., Hayun, L.B., Gruetter, C., Rauh, D., Ori, N., and Sessa, G. (2013). BSKs are partially redundant positive regulators of brassinosteroid signaling in Arabidopsis. Plant J. **74:** 905–919.

Tanaka, K., Asami, T., Yoshida, S., Nakamura, Y., Matsuo, T., and Okamoto, S. (2005). Brassinosteroid homeostasis in Arabidopsis is ensured by feedback expressions of multiple genes involved in its metabolism. Plant Physiol. **138:** 1117–1125.

Tang, W., et al. (2011). PP2A activates brassinosteroid-responsive gene expression and plant growth by dephosphorylating BZR1. Nat. Cell Biol. **13:** 124–131.

Tang, W., Kim, T.-W., Oses-Prieto, J.A., Sun, Y., Deng, Z., Zhu, S., Wang, R., Burlingame, A.L., and Wang, Z.-Y. (2008). BSKs mediate signal transduction from the receptor kinase BRI1 in Arabidopsis. Science **321:** 557–560.

Tian, Y., et al. (2018). Hydrogen peroxide positively regulates brassinosteroid signaling through oxidation of the BRASSINAZOLE-RESISTANT1 transcription factor. Nat. Commun. **9:** 1063–13.

van Esse, W., van Mourik, S., Albrecht, C., van Leeuwen, J., and de Vries, S. (2013). A mathematical model for the coreceptors SOMATIC EMBRYOGENESIS RECEPTOR-LIKE KINASE1 and SOMATIC EMBRYOGENESIS RECEPTOR-LIKE KINASE3 in BRASSINOSTEROID INSENSITIVE1-mediated signaling. Plant Physiol. **163:** 1472–1481.

Vert, G., and Chory, J. (2006). Downstream nuclear events in brassinosteroid signalling. Nature **441:** 96–100.

Vida, T.A., and Emr, S.D. (1995). A new vital stain for visualizing vacuolar membrane dynamics and endocytosis in yeast. J. Cell Biol. **128:** 779–792.

Vriet, C., Russinova, E., and Reuzeau, C. (2013). From squalene to brassinolide: The steroid metabolic and signaling pathways across the plant kingdom. Mol. Plant **6:** 1738–1757.

Wang, C., et al. (2013). Identification of BZR1-interacting proteins as potential components of the brassinosteroid signaling pathway in Arabidopsis through tandem affinity purification. Mol. Cell. Proteomics **12:** 3653–3665.

Wang, X., and Chory, J. (2006). Brassinosteroids regulate dissociation of BKI1, a negative regulator of BRI1 signaling, from the plasma membrane. Science **313:** 1118–1122.

Wang, R., Liu, M., Yuan, M., Oses-Prieto, J.A., Cai, X., Sun, Y., Burlingame, A.L., Wang, Z.-Y., and Tang, W. (2016). The brassinosteroid-activated BRI1 receptor kinase is switched off by dephosphorylation mediated by cytoplasm-localized PP2A B' subunits. Mol. Plant **9:** 148–157.

Wang, W., Bai, M.-Y., and Wang, Z.-Y. (2014). The brassinosteroid signaling network-a paradigm of signal integration. Curr. Opin. Plant Biol. **21:** 147–153.

Wang, X., Kota, U., He, K., Blackburn, K., Li, J., and Goshe, M.B. (2008). Sequential transphosphorylation of the BRI1/BAK1 receptor kinase complex impacts early events in brassinosteroid signaling. Dev. Cell **15:** 220–235.

Wang, Z.-Y., Bai, M.-Y., Oh, E., and Zhu, J.-Y. (2012). Brassinosteroid signaling network and regulation of photomorphogenesis. Annu. Rev. Genet. **46:** 701–724.

Wilma van Esse, G., Westphal, A.H., Surendran, R.P., Albrecht, C., van Veen, B., Borst, J.W., and de Vries, S.C. (2011). Quantification of the brassinosteroid insensitive1 receptor in planta. Plant Physiol. **156:** 1691–1700.

Winter, D., Vinegar, B., Nahal, H., Ammar, R., Wilson, G.V., and Provart, N.J. (2007). An "electronic fluorescent pictograph" browser for exploring and analyzing large-scale biological data sets. PLoS One **2:** e718.

Xu, W., Huang, J., Li, B., Li, J., and Wang, Y. (2008). Is kinase activity essential for biological functions of BRI1? Cell Res. **18:** 472–478.

Yang, C.-J., Zhang, C., Lu, Y.-N., Jin, J.-Q., and Wang, X.-L. (2011). The mechanisms of brassinosteroids' action: From signal transduction to plant development. Mol. Plant **4:** 588–600.

Yang, J., Roe, S.M., Cliff, M.J., Williams, M.A., Ladbury, J.E., Cohen, P.T.W., and Barford, D. (2005). Molecular basis for TPR domain-mediated regulation of protein phosphatase 5. EMBO J. **24:** 1–10.

Yin, Y., Wang, Z.-Y., Mora-García, S., Li, J., Yoshida, S., Asami, T., and Chory, J. (2002). BES1 accumulates in the nucleus in response to brassinosteroids to regulate gene expression and promote stem elongation. Cell **109:** 181–191.

Yoo, S.-D., Cho, Y.-H., and Sheen, J. (2007). Arabidopsis mesophyll protoplasts: A versatile cell system for transient gene expression analysis. Nat. Protoc. **2:** 1565–1572.

Yu, X., Li, L., Zola, J., Aluru, M., Ye, H., Foudree, A., Guo, H., Anderson, S., Aluru, S., Liu, P., Rodermel, S., and Yin, Y. (2011). A brassinosteroid transcriptional network revealed by genome-wide identification of BESI target genes in *Arabidopsis thaliana*. Plant J. **65:** 634–646.

Zhang, Y. (2008). I-TASSER server for protein 3D structure prediction. BMC Bioinformatics **9:** 40.

Zhang, Y., Liu, Z., Wang, J., Chen, Y., Bi, Y., and He, J. (2015). Brassinosteroid is required for sugar promotion of hypocotyl elongation in Arabidopsis in darkness. Planta **242:** 881–893.

Zhang, Z., Zhu, J.-Y., Roh, J., Marchive, C., Kim, S.-K., Meyer, C., Sun, Y., Wang, W., and Wang, Z.-Y. (2016). TOR signaling promotes accumulation of BZR1 to balance growth with carbon availability in Arabidopsis. Curr. Biol. **26:** 1854–1860.

Zhu, J.-Y., Li, Y., Cao, D.-M., Yang, H., Oh, E., Bi, Y., Zhu, S., and Wang, Z.-Y. (2017). The F-box protein KIB1 mediates brassinosteroid-induced inactivation and degradation of GSK3-like kinases in Arabidopsis. Mol. Cell **66:** 648–657.